Review article **Open Access**

Shiyi Xiao, Jiarong Wang, Fu Liu, Shuang Zhang, Xiaobo Yin* and Jensen Li*

Spin-dependent optics with metasurfaces

DOI 10.1515/nanoph-2016-0121
Received May 31, 2016; revised August 10, 2016; accepted August 17, 2016

Abstract: Optical spin-Hall effect (OSHE) is a spin-dependent transportation phenomenon of light as an analogy to its counterpart in condensed matter physics. Although being predicted and observed for decades, this effect has recently attracted enormous interests due to the development of metamaterials and metasurfaces, which can provide us tailor-made control of the light-matter interaction and spin-orbit interaction. In parallel to the developments of OSHE, metasurface gives us opportunities to manipulate OSHE in achieving a stronger response, a higher efficiency, a higher resolution, or more degrees of freedom in controlling the wave front. Here, we give an overview of the OSHE based on metasurface-enabled geometric phases in different kinds of configurational spaces and their applications on spin-dependent beam steering, focusing, holograms, structured light generation, and detection. These developments mark the beginning of a new era of spin-enabled optics for future optical components.

Keywords: geometric phase; metamaterials; metasurfaces; optical spin-Hall effect; spin-orbit interaction.

1 Introduction

Spin-Hall effect (SHE) is the physical phenomenon associated with the spin-dependent trajectories of electric current due to spin-orbit interaction. It can be either induced by extrinsic mechanisms from impurity scattering [1–3] or induced by intrinsic mechanisms, which have a geometrical origin from the spin-dependent Berry phase defined in the momentum space of the interested materials [4]. The discovery of SHE paves a unique way to manipulate particles by spin degree of freedom and opens up the research area of spintronics. Interestingly, the geometric origin of intrinsic SHE allows the discussion of spin-dependent phenomena extended to optics [5–12]. In this case, the two circular polarizations can be regarded as the two spins, and the appearance of spin splitting of light based on the spin-dependent Berry phase can be regarded as the optical analogy of SHE in condensed matter physics. It is proposed and experimentally demonstrated as what we now commonly refer as the optical SHE (OSHE) in showing a transverse spin-split of light trajectory [5–21]. These works can actually be traced back to the early works about the Berry phase for photons [22–26], which have triggered a series of developments to manipulate light and to study geometric phases using helical fibers [23–26], gratings [27–29], and liquid crystals [30–32]. More recently, the appearance of metamaterials allows us to have very flexible optical properties by building up artificial atoms with tailor-made responses at will, with the most prominent applications such as negative refraction [33, 34] and invisibility cloaks [35, 36] to practical applications such as flat lens [37, 38] and polarization control [39, 40]. The implications are two-fold. In one aspect, metamaterials provide us a flexible platform to study OSHE and then to explore different regimes of OSHE, for example, the OSHE in plasmonic systems, which are not easily achievable using conventional approaches. In another aspect, we can exploit OSHE as a useful resource for designing optical components and systems, which can take advantage of the spin degree freedom of light. We are witnessing a rapid development of spin-enabled optics based on the principle of OSHE and it is the purpose of the current article to give an overall review on the above two aspects. There are also other routes to carry out polarization/spin-dependent optics, similar to the case of SHE that there are other extrinsic/intrinsic mechanisms [41–44]. However, we here focus on the intrinsic OSHE relying on geometric phases, and the associated applications are very intuitive in design, giving opposite and automatic spin dependence in functionalities. This route also gives rise to devices with robust operation due to its geometric origin.

***Corresponding authors: Xiaobo Yin,** Department of Mechanical Engineering, University of Colorado, Boulder, CO 80309, USA; and Materials Science and Engineering Program, University of Colorado, Boulder, CO 80309, USA, e-mail: xiaobo.yin@colorado.edu; and **Jensen Li,** School of Physics and Astronomy, University of Birmingham, Birmingham B15 2TT, UK, e-mail: j.li@bham.ac.uk
Shiyi Xiao, Fu Liu and Shuang Zhang: School of Physics and Astronomy, University of Birmingham, Birmingham B15 2TT, UK
Jiarong Wang: Department of Mechanical Engineering, University of Colorado, Boulder, CO 80309, USA

Here, we give an overall review on the exciting developments on both the principles and the applications of OSHE enabled by the recent notion of metamaterials and metasurfaces [45–47], the one-atom-layer version of metamaterials. For a much broader perspective of spin-orbit interaction of light, Refs. [11, 12] provide useful resources. Here, we focus on introducing the applications of OSHE from different types of geometric phases. This paper is structured in the following sections. In Section 2, we briefly discuss and classify the principles in obtaining OSHE using geometric phases in different configurational spaces. It provides a unified view of OSHE and forms the basis in achieving the associated spin-dependent phenomena and applications in the following sections. Sections 3 and 4 are devoted to the realizations and observations of OSHE in the far- and near-field domains, respectively. The spin-dependent trajectories of light can be understood in terms of a splitting in the real space or in the momentum space. These form a basis for achieving more complicated splitting in beam structures and surface-wave control. In Section 5, we introduce the designer applications of OSHE enabled by a metasurface, including optical angular momentum detectors or generators, spin-dependent flat lens, holograms, and spin selection for other fundamental physical phenomena. Finally, we conclude in Section 6.

2 Basic principles of the intrinsic OSHE

The intrinsic OSHE can be understood as an effect arising from the spin-orbit interaction of electromagnetic waves: the polarization (spin) and the trajectory (propagation direction and phase) are affecting each other. The change of light's trajectory automatically accompanies a transverse spin-split of the beam center or a spin-dependent propagation phase occurs. Such a change of the trajectory can result from an inhomogeneous profile of refractive indices (n) or a sharp change of index on an interface [19]. In this case, the ∇n mimics the electric field in the conventional SHE. More vividly, it can be achieved by simply a curled optical fiber, where the light is forced to follow the fiber direction [6]. The change of the propagation direction can be alternatively viewed as a locus in the momentum state space, which is taken as the surface of a unit sphere, as shown in Figure 1A. When the state of light, with direction indicated by $\hat{k}$, undergoes a complete loop, the light picks up an additional geometric phase. This additional phase has geometric nature, as it is only related to the geometry of the state space. Suppose it is the left-handed circular polarization (LCP) under consideration, the state of the light with particular $\hat{k}$ can be described by its polarization $\psi=(\hat{\theta}+i\hat{\phi})/\sqrt{2}$, where $\hat{k}$, $\hat{\theta}$, and $\hat{\phi}$ define the usual right-handed local polar coordinate system on the curled fiber with the particular $\hat{k}$. The Berry connection A and the Berry curvature Ω can then be found as

$$\begin{aligned}\{A_\theta, A_\phi\}&=i\psi^*\cdot\{\partial_\theta\psi, \partial_\phi\psi\}=\{0, \cos\theta\}\\ \Omega&=\partial_\theta A_\phi-\partial_\phi A_\theta=-\sin\theta\end{aligned} \tag{1}$$

With these, the geometric phase is actually the integrated curvature defined by $\Phi_B=\int\Omega d\theta d\phi=-\int\sin\theta d\theta d\phi$, which can be interpreted as the surface area enclosed by the loop, shown as orange color in Figure 1A. The geometric phase, formally known as the Rytov-Vladimirskii phase [48–50], has the same magnitude but the opposite sign for the opposite polarizations. For an easier understanding, Ω can also be interpreted as an effective magnetic field,

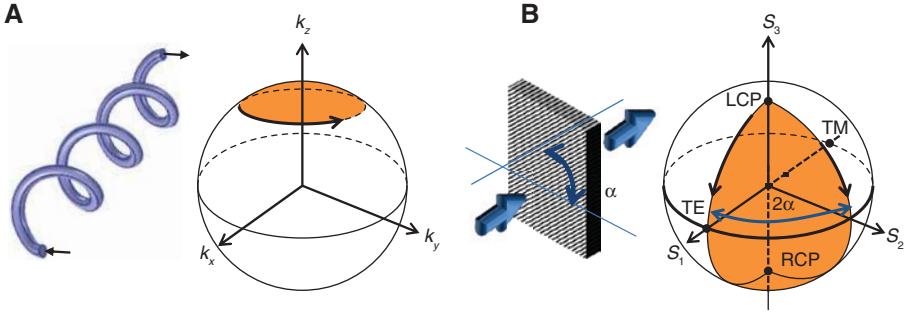

Figure 1: Geometric phases in different state spaces.
(A) Light propagation in a curled fiber associated with a geometric phase in the momentum space. (B) Light propagation across a half-wave plate, with orientation angle α for its fast axis, in turning LCP to RCP, associated with a geometric phase in the polarization space. The arrows on the materials or structures show the direction of light. The arrows on the state space show the directions of the light transport process.

curl of the Berry connection in the radial direction, which behaves like a magnetic monopole located at the origin of the *k*-space. The Berry connection can be interpreted as the vector potential in the momentum space. For the case of inhomogeneous refractive index profile mentioned earlier, such a geometric phase gives a reaction back to the trajectory of light beam. The equation of motion is then modified [6–8] by

$$\partial_t \boldsymbol{k} = -kc\nabla(1/n), \quad \partial_t \boldsymbol{r} = \frac{c}{n}\hat{k} \pm (\partial_t \boldsymbol{k}) \times \boldsymbol{\Omega}, \tag{2}$$

where the upper/lower sign indicates the opposite contribution for the two circular polarizations and *c* is the speed of light in vacuum, and the 3D Berry curvature vector from the "monopole" is defined as $\boldsymbol{\Omega} = \hat{k}/k^2$. It indicates the time evolution of the wave-vector $\boldsymbol{k}$ and wave-packet location $\boldsymbol{r}$. The first equation is the "force" formula, whereas the second equation is the velocity along the light trajectory. The effective magnetic field in the momentum space, in contrast to a magnetic field in real space, modifies the velocity formula, rather than giving a magnetic Lorentz force. It is a correction term beyond the classical optics limit and therefore gives rise to a spin-dependent splitting of ray trajectory usually in the order of wavelength [5–19].

The momentum space is not the only state space of light. Similar geometric phases and "magnetic monopole" of light can also be defined in another state space – the polarization space or the Poincaré sphere (see Figure 1B). In this case, a polarization state can be expressed as $\psi = \cos\frac{\theta}{2}|+\rangle + \sin\frac{\theta}{2}e^{i\phi}|-\rangle$ in terms of LCP $|+\rangle$ and right-handed circular polarization (RCP) $|-\rangle$. Correspondingly, the Berry connection and Berry curvature are

$$\{A_\theta, A_\phi\} = \left\{0, -\sin^2\frac{\theta}{2}\right\}, \quad \Omega = -\frac{1}{2}\sin\theta. \tag{3}$$

Therefore, a closed loop on the Poincaré sphere gives a geometrical phase $\Phi_B = \int \Omega d\theta d\phi = -\frac{1}{2}\int \sin\theta d\theta d\phi$, which is half of the enclosed area in this case. The geometric phase associated with the polarization space is called the Pancharatnam-Berry (PB) phase [51, 52]. The closed loop in Figure 1B actually consists of two possible routes from the north to the south poles on the Poincaré sphere. An example scenario is a half-wave plate in converting LCP to RCP, corresponding to two different orientations of the fast axis (two different orientation angles α) of the half wave plate, indicated by the arrows on the Poincaré sphere. Then, the phase difference between the two routes will be given by the discussed geometric phase, which is half of the enclosed area, i.e. $\Delta\Phi_B = \pm 2\Delta\alpha$ for the two spins. Indeed, unlike the geometric phase in the *k*-space, the geometric phase in the polarization space can be easily used in this "parallel" fashion. The geometric-phase profile can be encoded in a series of different local material orientations in parallel. It does not rely on a correction in geometric optics limit and can generate a very large beam-splitting, as discussed in Section 3.

With these examples of geometric phases, it becomes straightforward to discuss the origin of the different realizations of OSHE. The enabling key is the introduction of opposite geometric phases for the two spins/polarizations into a splitting of trajectory through spin-orbit interaction. In the case of the experiment by Hosten and Kwiat for a circularly polarized light beam entering a glass substrate [19], the different tangential wave-number *k* of the beam are refracted (forced to have a change of direction) into glass in parallel, picking up an additional geometric phase, which is proportional to the tangential wave-number but with opposite sign for the two spins. It uses the opposite geometric phases in the momentum space and creates a spin-split of the beam center in the transverse direction, in a very close analogy to the original SHE. In a later experiment [53], by shining a circularly polarized light on a chain of plasmonic particles with lattice or local anisotropy, the direction of the anisotropy selects a route from the north to the south pole in the polarization space (see Figure 1B). The introduced opposite geometric phases $\pm 2\alpha$ creates a spin-split of the transmitted light directions in this version of OSHE. With this background, it becomes not surprising that such a discussion of OSHE can be extended to a more generalized state-space of light. For example, when a circularly polarized light is coupled to surface plasmon polariton on a metal surface through a Bragg grating of circular shape, both the *k* direction and the spin (angular momentum) of light are changed when the surface wave is focused to the center [54, 55]. For the part of grating with orientation angle α, the combination of the change of *k* and spin renormalizes the original geometric phase from $\pm 2\alpha$ to $\pm\alpha$ (more details in Section 4). The above discussions form the basic framework in understanding all the OSHE phenomena in this article, from far- to near-field manipulation and from beam-splitting and direction splitting to the splitting of local orbitals. We regard any spin-splitting orbital phenomena based on the opposite geometric phases of the two spins as the intrinsic OSHE in a general context. As we shall see, we pay particular attention to the OSHE with metasurfaces by taking advantage of the excellent ability of metamaterial atoms in tuning the local spin-orbit interaction.

3 Observing OSHE in the far field

3.1 Transverse beam splitting with gradient-index metasurfaces

When light is refracted from air to a dielectric medium at an angle, the direction of light is changed, and the transversality of light imposes a requirement on the transportation of the polarization according to the equation of motion in the last section. The different *k*-components of the light evolve with an additional spin-dependent geometric phase, giving rise to a split of the beam center in the transverse direction in the early demonstrations, as shown in Figure 2A [18, 19]. With the recent introduction of metasurfaces, a completely refreshed look can be taken in OSHE as the metasurfaces provide a new way in bending light. To manifest the OSHE effect through a metasurface, we require the violation of inversion symmetry and the respect of the time-reversal symmetry. The time-reversal symmetry is naturally respected without involving magnetic optics or extrinsic OSHE. An inversion symmetry breaking metasurface, in its simplest version, is a single layer of "V-shaped" metamaterial atoms, which generate a linear gradient of local transmission phase profile [45–47]. Such a linear gradient of transmission phase profile, albeit a polarization conversion in the

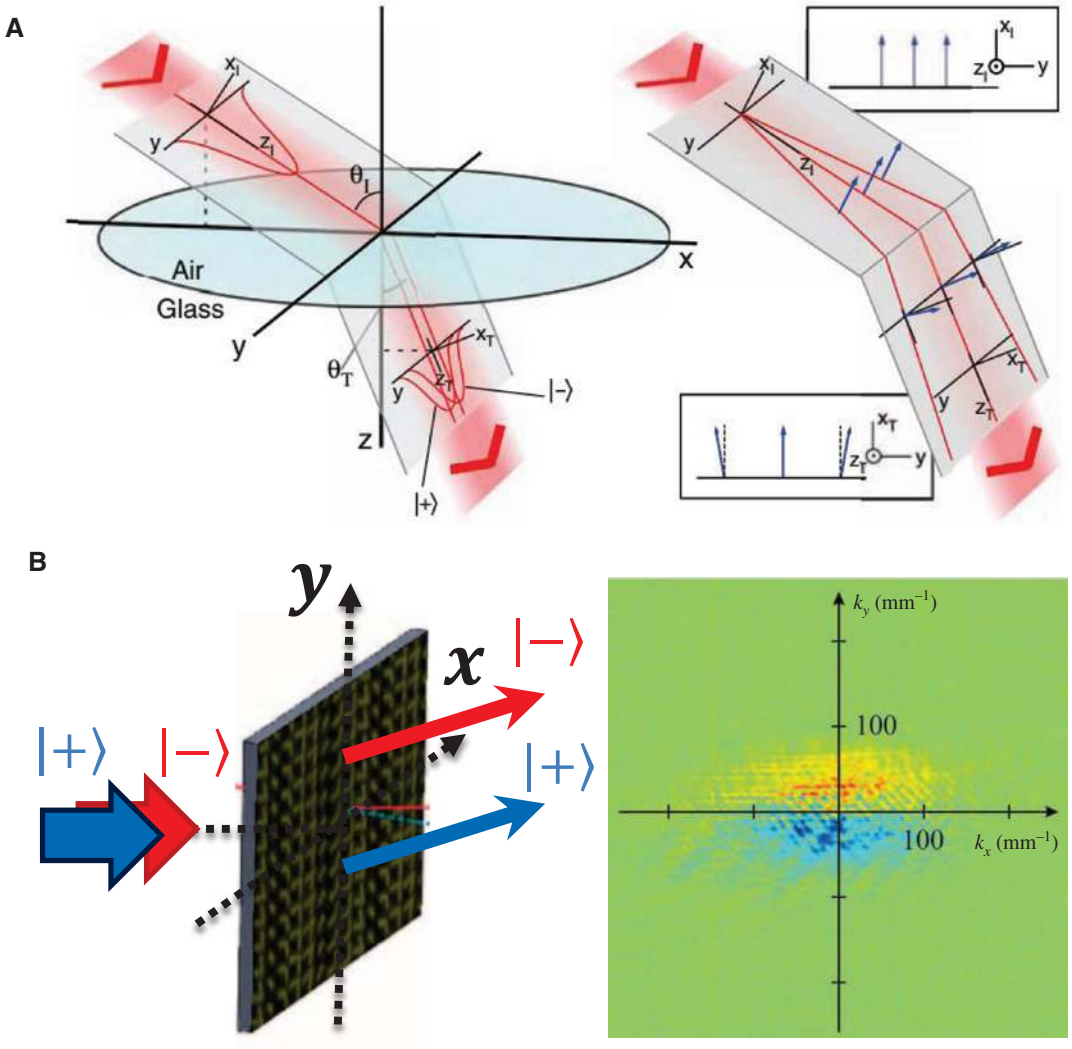

Figure 2: OSHE in giving transverse beam-splitting.
(A) Spin-splitting of beam center from air to glass at oblique incidence due to spin-dependent geometric phase picked up by different *k*-components. Reprinted from Ref. [19]. (B) OSHE at normal incidence using a metasurface, with the beam helicity (S_3 Stokes parameter) plotted on the right. Reprinted from Ref. [56].

transmission, bends the incident light from one side of the metasurface to the other side. Such a bending can have an arbitrarily designed angle much larger than the one given by an air-glass interface, giving rise to a spin-split of the beam center in the transverse direction. Such a scheme is summarized in Figure 2B with the beam helicity (the S_3 Stokes parameter) plotted as different colors representing the two spins [56]. Although the splitting may still be in the order of wavelength, it is much larger than the one given by previous approaches. Now, it can be easily detected by the measurement in the far-field regime and it can occur at normal incidence using a metasurface. By performing a quantum weak measurement [57–59] on the light field with the preselected and postselected position and helicity, one can further amplify the OSHE effect and the associated transverse transport of the light field [19, 60]. It is also worth noting that the pure electronic readout of OSHE has been recently proposed and demonstrated through the momentum transfer from the light field to the collective electron motion in the transverse direction [61]. In addition, the detection of the OSHE can be further improved using dielectric metasurfaces instead of the lossy metallic ones [62, 63]. Symmetry and symmetry breaking play a key role in OSHE. A respected time-reversal symmetry and a broken inversion symmetry of the discussed metasurface introduce a transverse motion of light beam, which has been mostly discussed in the literature. In addition, for a Gaussian beam with radial symmetry, the transverse motion can also be introduced in the azimuthal [64] and radial [65] directions by carefully engineering the spatial variation of the light-bending metasurfaces.

3.2 Linear and angular momentum splitting using geometric-phase metasurfaces

A move in the *k*-space, with a spin-dependent geometric phase to bend light, can be regarded as an OSHE. Similarly, a change of polarization also induces a geometric phase and it can be used to do an equivalent job. The polarization state of light can be easily altered by an anisotropic material, with its orientation angle α (see Figure 1B) to control the phase of the transmitted light. For an LCP incident light being converted to an RCP light, light propagation with two different orientation angles (α) follow two different paths from the north to the south pole of the Poincaré sphere. The phase difference between the two routes is simply half of the enclosed area, being called the PB phase. This fact can be simply derived by considering the rotation of coordinate frame between the laboratory coordinates (x,y) and the principal coordinates (u,v) of the anisotropic material. An incident LCP can be written in the material frame as $\hat{x}+i\hat{y}=e^{i\alpha}(\hat{u}+i\hat{v})$, whereas the transmitted RCP can be written as $\hat{x}-i\hat{y}=e^{-i\alpha}(\hat{u}-i\hat{v})$. Therefore, the transmission phase from LCP to RCP in the laboratory frame can be simply understood as the corresponding one in the material frame with an addition of geometric phase 2α [66, 67]. This geometric phase only occurs for the cross-polarized transmission and has its sign flipped for RCP to LCP conversion. It can be summarized as $2\sigma\alpha$, where $\sigma=+1$ with LCP incidence and $\sigma=-1$ for RCP incidence. Instead of transforming the different *k*-components with a geometric-phase profile in a parallel fashion in the last section, now we can directly transform the wave front at different positions, again in a parallel fashion, by having a spatially inhomogeneous profile of the material orientation, as long as the material response is anisotropic, giving a cross-polarized transmission. For example, one can design the orientation profile to be a linear profile $\sigma=(\Delta k)\cdot x/2+\alpha_0$, where Δk is interpreted as the momentum imparted by the inhomogeneous material. According to the generalized Snell's law of a metasurface [45–47], the transmitted light travels to two off-normal directions depending on the input spin by

$$k_x = k_{x,0} \pm \Delta k, \tag{4}$$

where $k_x(k_{x,0})$ is the transverse wave-number of the transmitted (incident) wave. Here, the upper (lower) sign indicates the situation for an LCP (RCP) incidence. The OSHE is then revealed as a symmetric spin-splitting of the propagating direction, or linear momentum, due to the opposite geometric phases of the two spins. Figure 3A shows the first experiment in revealing such an OSHE using a chain of localized plasmonic coaxial nanoaperture. In this case, the anisotropy comes from the coupling between neighboring particles. The tangent line between neighboring particles represents the previously introduced orientation α. The corresponding spin-splitting of the linear momentum is shown in Figure 3A [53]. Conventionally, the different orientations of local anisotropy can be obtained using quasi-periodic diffraction grating structures [27–31]. Using metasurfaces, the local orientations of the metamaterial atoms (the anisotropy) can now be individually controlled, leading to a more intuitive local control of the geometric-phase profile. The inset of Figure 3B shows a monolayer of subwavelength plasmonic nanorods with strong local anisotropy on a metasurface. The linear geometric-phase profile is obtained by locally rotating the rods, of orientation angle α, also in a linear fashion [67–70], found as $\Phi_B=\pm 2\alpha$. As the phase shift only relies on direction of local nanorods, the

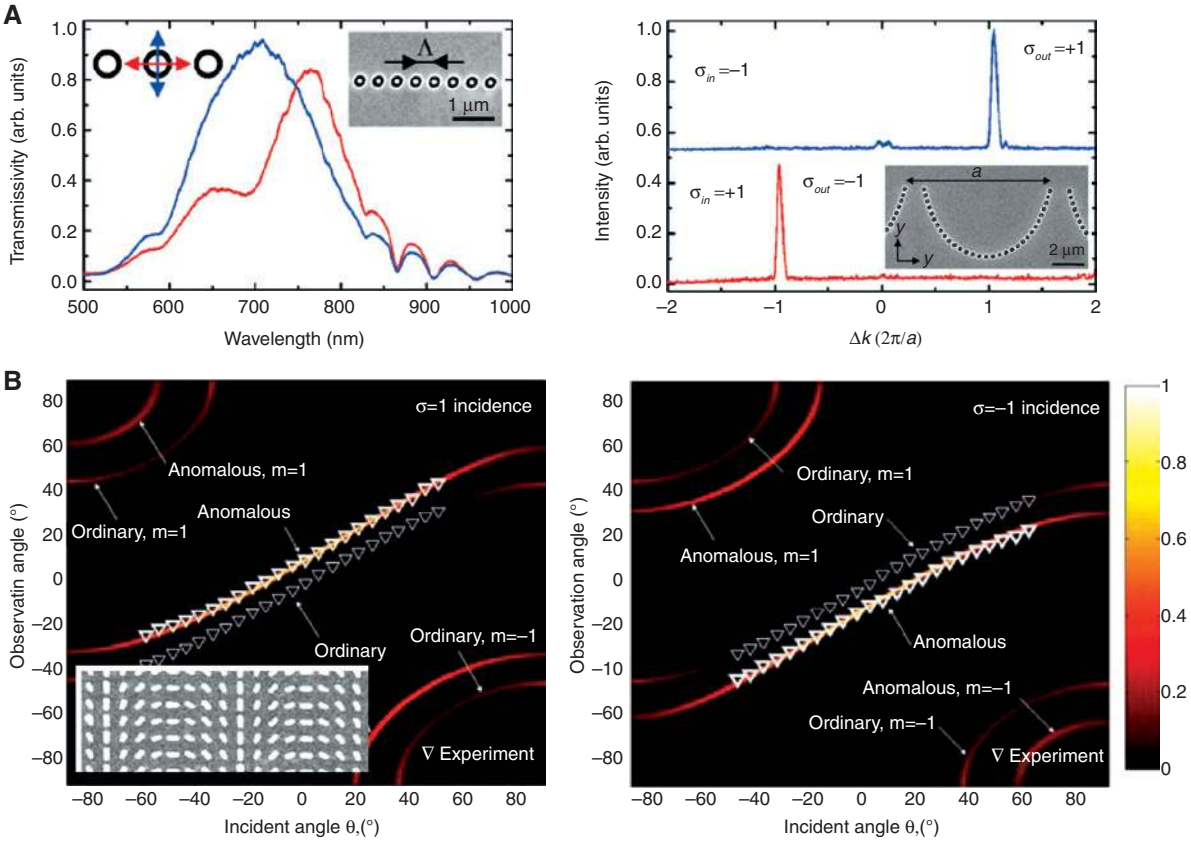

Figure 3: Spin splitting in linear momentum space.
(A) Isotropic coaxial nanoapertures chain for SHE. Left: Transmission spectra of the plasmonic chain showing anisotropy for linear polarization along two orthogonal directions due to the coupling of neighboring particles. Right: Spin-dependent momentum redirection for the OSHE. Inset: SEM image of a curved chain. Reproduced from Ref. [53]. (B) Anisotropic nanorod array for OSHE. Left (Right): Measured reflection angle versus incident angle for $\sigma=1$ ($\sigma=-1$) incidence, respectively. Inset: SEM image of nanorods fabricated on an ITO-coated glass. Reproduced from Ref. [68].

spin-dependent Δk is wavelength independent, whereas the outgoing angle depends on different wavelengths (see Figure 3B). This type of metasurfaces can be called geometric-phase metasurfaces.

Apart from demonstrating a spin-splitting of linear momentum, such a geometric phase in polarization space can also be used to manipulate the orbital angular momentum (OAM) of the transmitted light. A beam with OAM possesses a helical wave-front comprising an azimuthal profile $\propto\exp(il\Phi)$. Here, Φ is the azimuthal angle and l is an integer, simply called the OAM of the beam [71–74]. Early works on generating OAM relied on using locally anisotropic dielectric half-wave plates [28, 29]. Similar to the previous case, spin is flipped in the transmission together with an additional geometric-phase profile $\pm 2\alpha$ but now is designed as a linear profile of the azimuthal angle: $\alpha=q\Phi+\alpha_0$. q is called the topological charge of the material and α_0 is the initial orientation at zero angle. The orientation profile α then impacts the opposite geometric-phase profile ($\pm 2\alpha$) for the two spins on the incident wave-front, which now acquires a change of OAM by

$$l'=l+2\sigma\partial_\varphi\alpha=l+2\sigma q. \tag{5}$$

For example, when a light with zero OAM passes through a $q=1/2$ plate, the transmitted beam acquires an OAM of $l=\pm 1$ (see Figure 4A) [75]. These two beams of different OAMs only have difference in their phase but not the amplitude profile. They can be analyzed by an additional refractive helical phase plate, in which a unit of OAM is added to the output, giving resultant $l=0$ and 2 for the two different incident spins, as shown in the same figure. A signature of the nonzero OAM is a singularity spot at the beam center of undefined phase and zero amplitude. In fact, if we just want to show the spin-splitting to reveal the OSHE, we can use the residual beam, the copolarization transmission without geometric phase, as a reference beam. In this case, the metasurface consists of slits with $q=1$, which does not need to behave locally as half-wave plates [76, 77]. The resultant interference pattern from a

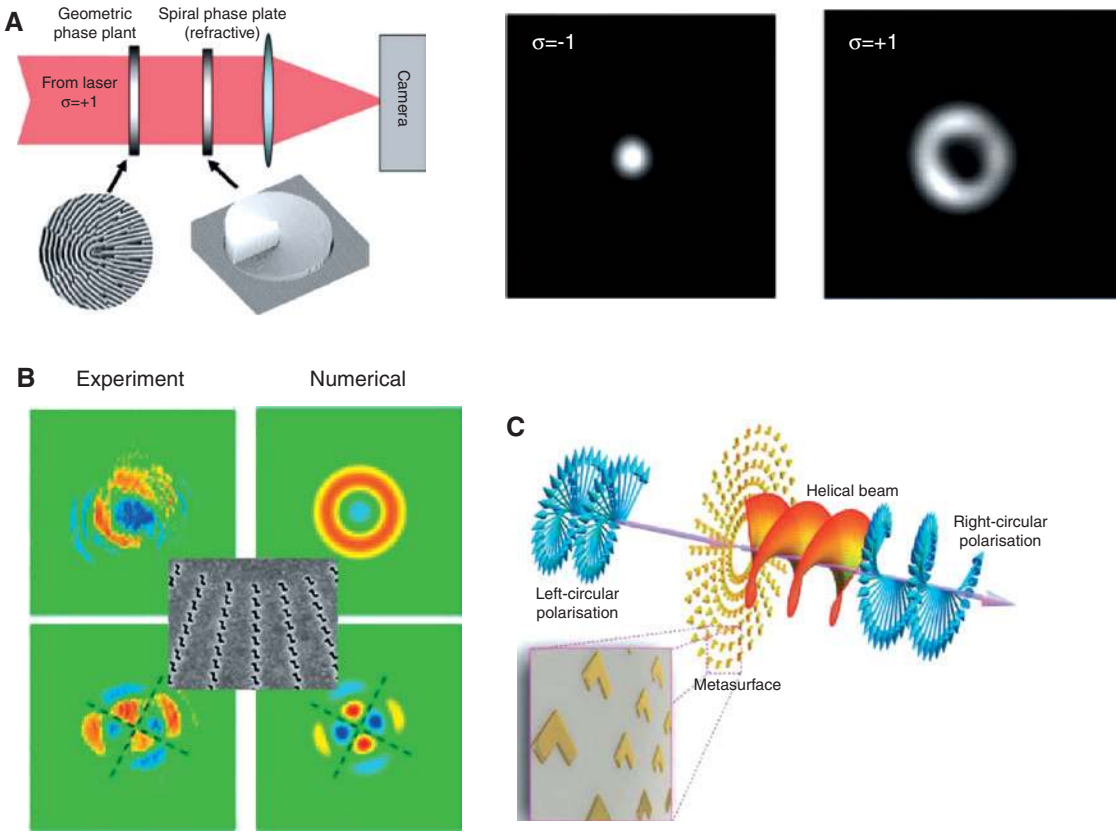

Figure 4: Spin splitting in angular momentum space.
(A) Measuring an $l=\pm 1$ vortex beam from a diffraction q-plate using a spiral wave plate. Measured intensity distributions are shown on the right. Reproduced from Ref. [75]. (B) Metasurface for spin-induced manipulation of OAM. Measured (left column) and numerical (right column) Stokes parameter S_3 with RCP incident light (top row) and linear polarized incident light (bottom row). Inset: SEM image of metasurface sample. Reprinted from Ref. [76]. (C) Vortex beam generator using spin-to-orbit coupling through a metasurface. Reprinted from Ref. [77].

linear polarized incident beam (consisting of both spins) shows a spin-splitting in the far-field, as illustrated in the measured Stokes parameter S_3 in Figure 4B. The two different colors represent the two different spins in the figure. The observed orbital rotation from the x-y axes results from the nonzero α_0 at zero azimuthal angle, as the slits are actually zigzag in shape. In these examples, the spin angular momentum is transferred to the OAM of the transmitted beam. Based on these simple versions of metasurfaces, more spin-dependent phenomena in orbital momentum were proposed [63, 68, 78–81], such as, for example, far-field spin-dependent focal point splitting [79], controllable OSHE with large OAM [80], OSHE with rotational symmetry breaking [63], OAM-focusing lens [81].

As metasurfaces are much thinner than a wavelength, diffraction from neighboring "pixels" is not severe; therefore, the resolution of the control of the geometric-phase profile can be very high, only limited by the size of individual metamaterial atoms. On the contrary, the efficiency of converting to the cross-polarization can be easily controlled by tuning the resonating response of the individual atoms, alongside the high resolution of the geometric-phase control. The residual beam, the one not carrying geometric phase, is therefore minimized in its intensity. With optimal design in the transmission geometry, almost 25% efficiency can be achieved by a single-layer nonmagnetic metasurface (see Figure 5A) [82]. Based on the use of three anisotropic sheet metasurfaces (see Figure 5B) [83, 84] cascaded along the direction of propagation, the control of vector Bessel beams is proposed with very high efficiency (a beam generator with 20 dB) due to the added magnetic response in the geometric-phase metasurface. In the reflection geometry with a ground plane, magnetic response is already embedded and almost 100% efficiency (see Figure 5C and D) can be obtained in steering the reflected beam against the specular reflection of the residual beam [85, 86]. These works based on plasmonic particles and metasurfaces have paved a unique way to achieve OSHE in both the visible and the infrared regimes,

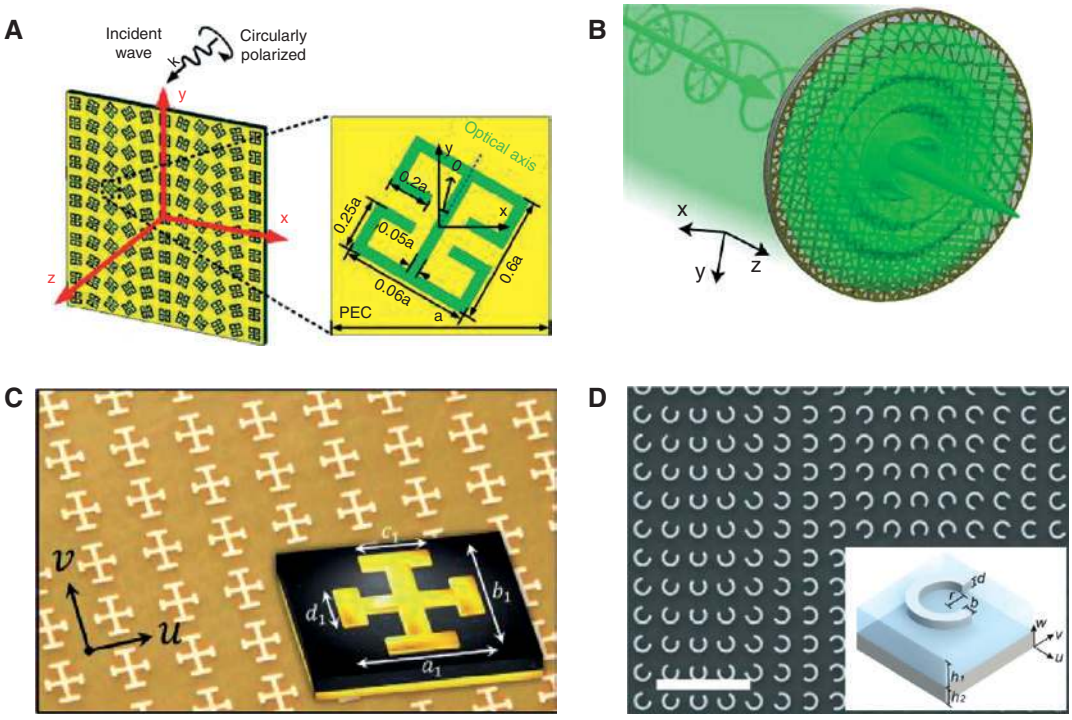

Figure 5: High efficiency geometric-phase metasurfaces.
(A) High-efficiency geometric-phase metasurface in transmission geometry. Reprinted from Ref. [82]. (B) High-efficiency vector Bessel beams generator. Reprinted from Ref. [83, 84]. (C and D) Almost perfect OSHE in reflection geometry working in microwave and tetrahertz region. (C and D) Reprinted from Refs. [85, 86], respectively.

resulting from the discussed opposite geometry phases for the two incident spins.

4 Observing OSHE in the near field

When an incident wave carries angular momentum and is converted to a surface plasmon on a metal surface, light suffers both a momentum redirection and a polarization change [54]. As we shall see in the examples when the orientation α is bound to the propagation direction of the surface plasmon, it renormalizes the original geometric phase from $\pm 2\alpha$ to $\pm\alpha$. This section presents a review on these near-field SHE, from individual scatterers to nano-antenna arrays. The observed SHE are usually revealed as focal spot splitting or a flipping in the propagating direction due to the opposite geometric phase for two spins. We also see a more complicated control later.

4.1 Surface plasmon generation with a single scatterer

Interestingly, OSHE in the near field can occur when the incident light illuminated even on a single isotropic scatterer [87]. Figure 6A shows a circular slit that is used to scatter a circularly polarized light in the far field into an outgoing surface plasmon, which can be described by a scalar wave E_z. By considering a rotation of the coordinate frame of the incident polarization, one can easily derive that the surface wave bears an angular phase profile $e^{i\sigma\Phi}$. This spin-dependent geometric-phase profile can be regarded as an optical vortex with unit OAM. Figure 6B shows the measured spin-dependent fringes by interference with a reference surface-wave generated from a long rectangular slit at the same time [87].

The converse situation will be scattering on a circular nanoslot in focusing the surface wave into its center, as shown in Figure 6B. It is a summation of surface waves from each local portion of the slit at an orientation angle α in a radiating direction perpendicular to the slit. A rotation of coordinate frame then connects these different cases together, giving rise to a geometric phase of $\pm\alpha$. This is different from the geometric phase of $\pm 2\alpha$ in the far-field situation. By putting $\alpha = \Phi$ to represent the orientation of the slits at different azimuthal angles, we immediately arrive that the focusing surface wave should be $e^{i\sigma\Phi}$, with an OAM of ± 1. When we consider a semicircular arc for the slot instead of a full circle, this angular profile of geometric

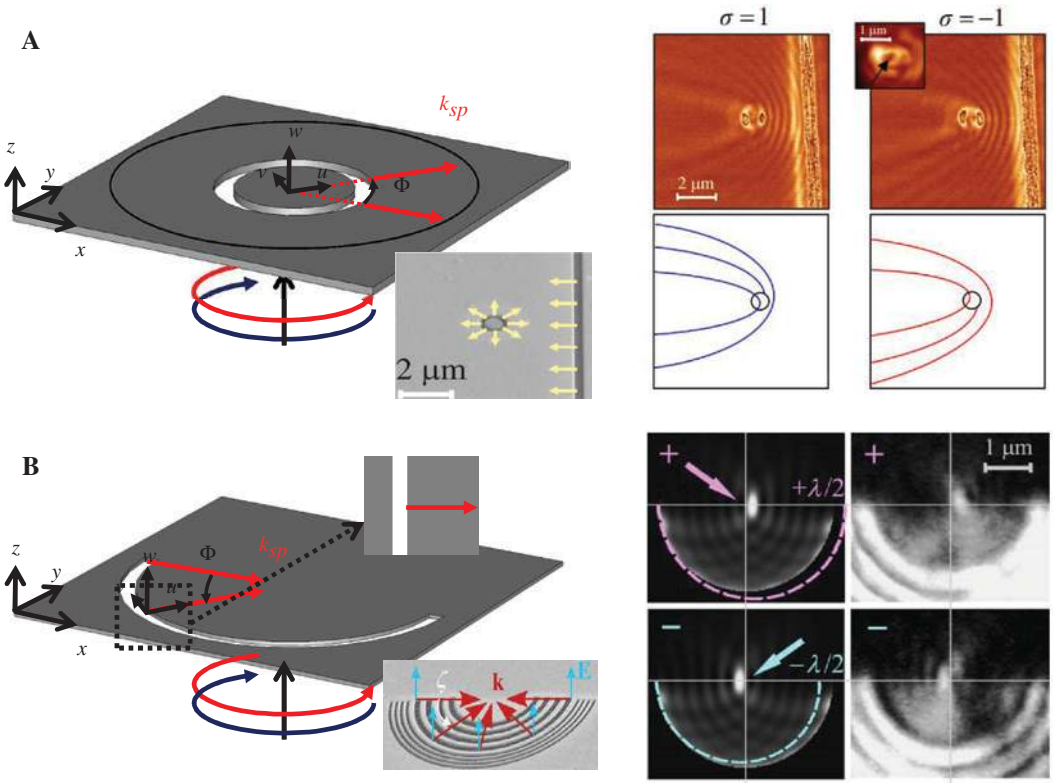

Figure 6: SPP generation by circular slit.
(A) Circular nanoslot in generating spin-dependent outgoing surface waves. Interference fringes between the surface wave with a traveling plane wave for the two CP incidences are shown on the right. Reprinted from Ref. [87]. (B) Semicircular nanoslot in focusing surface waves. The spin-splitting of the focal spot is shown on the right. Reprinted from Ref. [54].

phase induces a transverse shift of the focal point, either $\lambda_{SPP}/2$ or $-\lambda_{SPP}/2$, depending on the incident spin, where λ_{SPP} is the wavelength of the surface wave [54, 55].

It is interesting to note that the spin angular momentum of the light is completely converted into the OAM of the surface waves, or viewed as a conservation of the total angular momentum, for the case of isotropic defect with rotational symmetry. More spin-dependent phenomena can be achieved by employing chiral plasmonic structures with embedded topologic charge. Figure 7A shows the schematic diagram of the Archimedes spiral [88–95]. The topological charge $q = -1$ for the structure is defined by the rate change of radius against azimuthal angle: $r = r_0 - \lambda_{SPP} q\Phi/2\pi$. Because each local part of the spiral nanoslot (located at r) can be approximated to a circular structure with radius r (like in the last subsection), the surface plasmon propagating towards the center of spiral has a phase profile of $\sigma\Phi$. In addition, the surface wave from different portions of the spiral slit arrives at the center with different spin-independent dynamic phases due to the increasing radius. As a result of these two effects, the total phase gained from this consideration is Φ_{SPP}, which can be expressed as

$$\Phi_{SPP} = l_{SPP}\phi = (\sigma + q)\phi, \tag{6}$$

where l_{SPP} is the OAM of surface plasmon arriving the center. In this case, the additional angular momentum is provided by the topological charge of the spiral plate. However, unlike the far-field examples in Section 3.2, the contribution of the topological charge is spin independent. Figure 7B illustrates the amplitude and the phase of the surface wave when the structure is excited by a circularly polarized plane wave. The OAM of the surface wave is modified by the topological charge according to Eq. (6), now with a phase singularity and a dark spot at the center. We also note that the value of OAM is related to the radius of the dark spot, which can be directly measured by the standard near-field measurement technique (see Figure 7C) [55, 89]. Such a spin-dependent SPP profile can be further exploited to achieve a spin-dependent transmission filter through an array of coaxial nanoapertures [90], as shown in Figure 7D. In this case, the spiral has a topological charge $q = -2$, being added to the incident angular momentum $\sigma = \pm 1$, to excite the surface waves. The OAM of the surface wave becomes $l_{SPP} = -1$ (–3) for LCP (RCP) incidence and it has to match with the coaxial

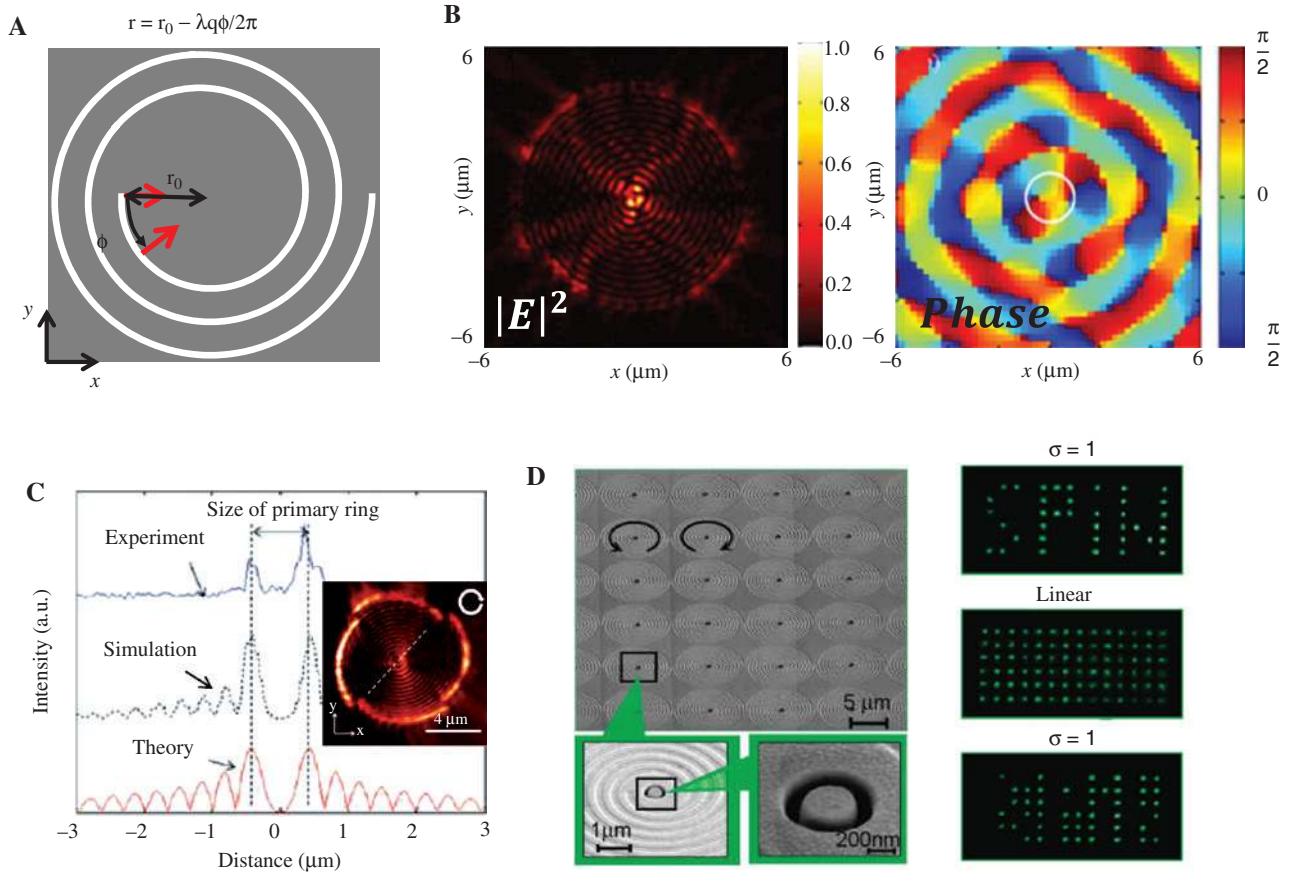

Figure 7: Spiral structures for OAM control in near field.
(A) Schematic diagram of the Archimedes spiral in generating surface plasmon. (B) Electric field of the generated surface plasmon on a metal surface. Reprinted from Ref. [88]. (C) Near-field measurement of the OAM of the generated surface plasmon. Reprinted from Ref. [89]. (D) Spin filter with each pixel consisting a spiral with a coaxial nanoaperture. Measured spin-dependent transmission through the array is shown on the right. Reprinted from Ref. [90].

aperture beneath and at the center of each spiral, which only allows a mode of OAM of ±1 to pass through. The combined effect is shown in Figure 7D. The word "SPIN" is obtained in transmission for one kind of circular polarization incidence but not the other with a huge contrast due to the mismatch of angular momentum [90].

4.2 Surface plasmon generation with geometric-phase metasurfaces

The previous structure with definite topological charge (e.g. circular or spiral nanoslots) provides a spin-orbit coupling between the incident spin and the generated surface plasmon. Actually, such a spin-orbit coupling can also occur even for a scatterer with other shapes in scattering the incident light to surface plasmon. Figure 8A shows an example of a single slit illuminated by a tightly focused linearly or elliptically polarized light beam [96]. The shift in either the focal point or the direction of the generated surface waves is measured using a "weak measurement" approach. Spin-splitting can also be directly observed using circularly polarized light as incidence as an asymmetric excitation of surface plasmon propagating towards the left- and right-hand sides of the slit. When an appropriate angle of incidence is chosen, the asymmetry is optimal and is revealed as a spin-dependent unidirectional excitation of the surface plasmon (see Figure 8B and C) [97–99]. Moreover, such asymmetric effects can be demonstrated for even a single particle placed on the surface of metal surface [98–100]. As a direct implication, the particle is optically pushed in opposite directions for the incidence of different circular polarizations as demonstrated as the mechanical effects from spin-orbit coupling [101, 102].

When the slit becomes much smaller than a wavelength, it reradiates as a localized dipole moment [100]. In this case, a circular polarization incidence $(\hat{x}+i\sigma\hat{y})$ generates a "spin-flipped" dipole moment $\vec{p}=e^{i2\sigma\alpha}(\hat{x}-i\sigma\hat{y})$, where α is the orientation of the slit measured from the x-axis. The surface plasmon reradiated from this dipole,

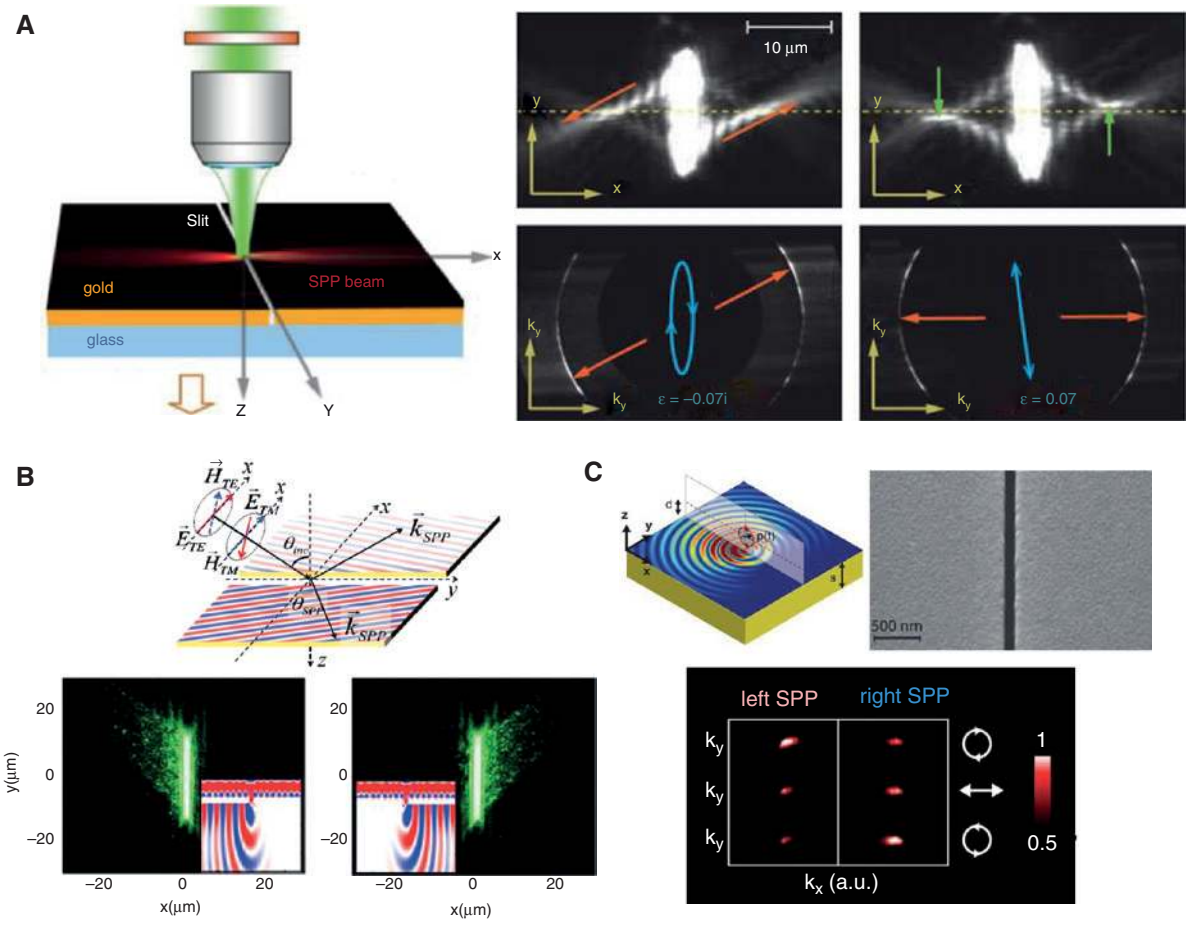

Figure 8: OSHE on a single nanoslot.
(A) Observation of the spin-dependent shifting of scattered surface plasmon from a single nanoslot using the weak measurement approach. Left: Scheme of the experimental set-up. Right: SPP field distributions in real (top row) and Fourier spaces (bottom row) with different incident polarizations are shown in cyan. Reproduced from Ref. [96]. (B) Exciting surface plasmon with different circular polarization on a long slit. Reproduced from Ref. [97]. (C) Asymmetric SPP emission from a single nanoslot and nanoparticle (top row). Reproduced from Ref. [98].

a scalar wave (E_z), can be simply obtained by changing $\hat{x}/\hat{y}$ to $\cos\beta/\sin\beta$, where β is the azimuthal angle between the x-axis and the location of the surface wave to be evaluated sufficiently far away from the dipole (see Figure 9A). Therefore, the total phase carried by the surface-wave radiation for the spin-flipped component is

$$\Phi = \sigma(2\alpha - \beta), \tag{7}$$

where $2\sigma\alpha$ can be regarded as the same PB phase term with that in the far field. Here, by setting the radiation angle always perpendicular to the nanoslot ($\beta = \alpha$), the phase of spin-flipped component will become $\Phi = \sigma\alpha$. Such a geometric phase can also be interpreted by the Coriolis effect of light [54], where light suffers from both a momentum redirection and a polarization change when coupled into surface wave. On the contrary, for the radiation without spin-flipping, the geometric-phase factor 2α in the above formula is absent. As both terms radiate from the same dipole, the total radiation can be written as $e^{i\sigma\beta} + e^{i\sigma(2\alpha-\beta)} = 2e^{i\sigma\alpha}\cos(\alpha-\beta)$ where the $\sigma\alpha$ term is the geometric phase arisen from an interference of the "spin-flipped" and "spin-conserved" component. Figure 9B shows an array of slits. Each unit cell consists of two columns of nanoslits, one at orientation $\alpha = \pi/4$ and another at orientation $\alpha = -\pi/4$, with combined radiation in the horizontal direction [103]. Suppose it is an LCP ($\sigma = 1$) incidence. The right (left)-hand column of slits radiates with phase $-\pi/4$ ($+\pi/4$), according to Eq. (7). Together with a designed dynamic phase separation of $\pi/2$ between the two columns, the radiations are destructively (constructively) interfered to the right (left) in the horizontal direction. For an RCP incidence, the unidirectional propagation is in the opposite direction (see Figure 9B). The radiation pattern for such a unit cell is very anisotropic. The orientations of the slits are chosen to have $\cos\alpha$ invariant for the two horizontal directions so that the interference is between waves

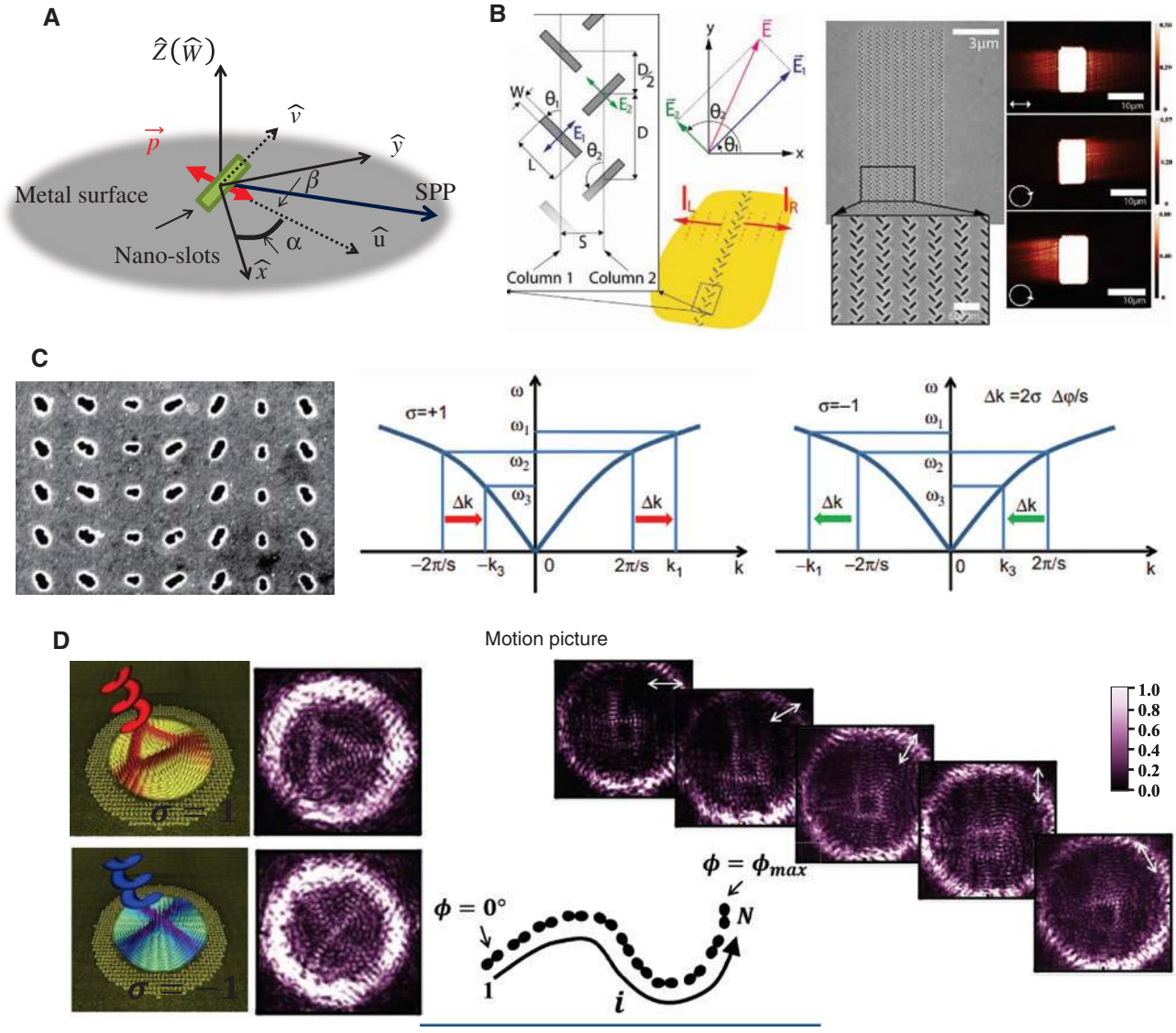

Figure 9: Spin-dependent trajectories enabled by nanoslots array.
(A) Schematic diagram in generating surface plasmon by a dipole source on metal surface. (B and C) Unidirectional propagation achieved by nanoslots, where B (C) employs coupled (single) nanoslots in one unit cell. (B and C) Reprinted from Refs. [103, 104], respectively. (D) Scheme of flexible coherent control of plasmonic SHE. Left: Independent generation of local orbitals for the two incident spins. Right: Motion picture generated by rotating a linear incident polarization in writing a letter "b". Reprinted from Ref. [105].

of the same magnitude. Such a slit (with dipolar radiation profile) array is very useful in tailoring the propagation of surface plasmon polaritons, for example, generating Cherenkov surface plasmon [106] and achieving spin-dependent transmission through decorated subwavelength aperture on plasmonic metal [107]. The appearance of the spin-flipping geometric-phase term involving $2\sigma\alpha$ in Eq. (7) is actually playing the key role in the phenomenon. The structure can be further simplified to a unit cell consisting of only one slit. In this case, the orientation profile α is designed as a linear function of x, as illustrated in Figure 9C [104]. For a periodicity of α in the x-direction, a unidirectional propagating surface plasmon can only be excited for a chosen incident spin σ by matching the momentum of surface waves: $k_{x,\,SPP} = 2\sigma\partial_x\alpha + m\,2\pi/a$, where the integer m is the chosen working diffraction order. As there is a mirror symmetry breaking in the geometric-phase profile 2α, the matching can only be fulfilled in a single direction. Such a consideration can also lead to more dispersion-related phenomena (e.g. Rashba-like effect in thermal radiation) [108–112], which will be introduced in Section 5.

The opposite geometric phases for the two spins are related to the various opposite spin-dependent shifts in the previous sections. These include a transverse shift of beam center, a shift in the linear momentum or the OAM of the incident beam, and a shift of focal spot from a

circular grating. For surface-wave excitation, this simple relationship between the two incident spins can actually be relaxed if we are only interested in generating local orbitals in a finite region. Figure 9D shows a platform with slits of a tailor-made orientation profile around a central slit-free region [105]. Another way to interpret Eq. (7) is that if we require neighboring slits contribute to a surface plane wave with phase Φ_B in a direction of angle $\beta = \arg(k_x + ik_y)$, we should set $\alpha = (\sigma\Phi_B + \beta)/2$. Therefore, by taking the holographic approach to generate a target profile E_z using constructive interference from all the slits, we change Φ_B to $\arg E_z$ and $k_{x(y)}$ to $\partial_{x(y)}$. Neighboring slits then contribute to the required local plane waves and we obtain $\alpha = \pm\frac{1}{2}\arg((\partial_x \pm i\partial_y)E_z)$ with an arbitrary global additive constant. Because we are only interested in the standing waves generated in the center region, we only require E_z to share in common with your actual target profile on the inward radiation part. We can therefore set $\alpha = \pm\frac{1}{2}\arg((\partial_x \pm i\partial_y)(E_z^+ + (E_z^-)^*))$, where E_z^+ and E_z^- represent the target profiles, which only include the inward radiation parts for the two spins separately. The target profiles for the two spins within the central region can then be specified individually without a simple relationship between them. Figure 10A illustrates the independent and flexible SHE: a cross (triangle) for LCP (RCP) incidence. Such flexible control of SHE enables the two spins to work together in a coherent way [116–118]. Motion pictures with a series of picture frames can be assembled and played by rotating a linear polarization as incidence, as shown in the same figure.

5 Application of OSHE and geometric-phase metasurfaces

With the OSHE demonstrated in the previous sections, there are numerous proposed applications by taking advantage of the associated spin-orbit interaction of light. Different spin-dependent optical elements and physical phenomena can be explored.

5.1 OAM generator and detector

Usually, the spin angular momentum and intrinsic orbital momentum of light are not easy to be measured. Conventional approaches use bulky free space components,

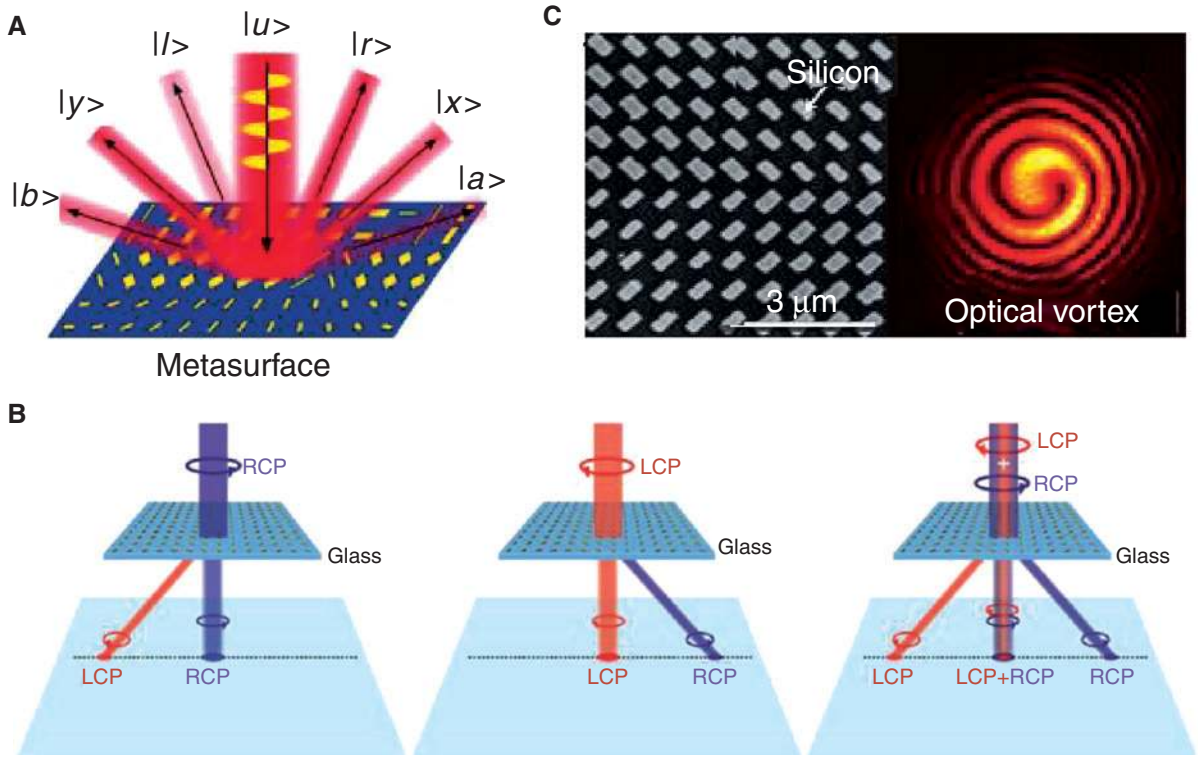

Figure 10: OAM generators and detectors.
(A and B) Geometric-phase metasurface in sorting different polarizations. Reprinted from Refs. [113, 114], respectively. (C) Generating optical angular momentum by metasurface. Reprinted from Ref. [115].

such as wave-plates and polarizing analyzers, diffraction gratings [119, 120], spatial light modulator [121–123], and interference measurement [124–127]. Spin-dependent metasurfaces, on the contrary, show a strong capability to generate and detect the angular momentum of light [113, 114, 128–130]. For example, a detector metasurface designed by holographic approach was proposed [128]. Only the incident light carrying the designed OAM can launch the particular surface plasmon with constructive interference. Similarly, using geometric metasurfaces with rotating slits or bars, a composite light beam with different spins or polarization states can be sorted into different directions in either reflection (see Figure 10A) and transmission (see Figure 10B) geometry [113, 114]. The ellipiticity of the incident light can also be analyzed. The geometric-phase route has an advantage of being robust against fabrication impurities. On the contrary, the generation of vortex beams is critical for fascinating applications ranging from super-resolution imaging techniques such as stimulated emission depletion (STED) microscope to high-bandwidth quantum information processing. Space-variant metasurfaces have been widely adopted to generate and manipulate the OAM of light in a precise and versatile manner (see Figure 4C). More realistic approaches were proposed based on dielectric metasurfaces made of silicon (or TiO_2) cut-wires to obtain a high conversion efficiency and a low ohmic loss (Figure 10C) [115].

5.2 Geometric phase enabled planar lens and holograms

Although OSHE has been observed for decades, only simple splitting in the real space and in the momentum space has been demonstrated until not long ago [19, 53–56]. This is partly due to the fact that only simple structures and materials can be employed in fabrication previously. The resultant geometric-phase profile is relatively simple. Recently, metasurfaces with anisotropic nanostructures provide a straightforward approach to achieve arbitrary geometric-phase profiles with high resolution simply by rotating the nanostructures [67–70]. The associated OSHE opens a new gateway to more flexible spin-dependent optics. For example, a spin-dependent metasurface lens can be fabricated with an orientation of the structures with quadratic profile. Such a lens can be switched from a focusing to a diverging lens simply by changing the incident light from one spin to another [131–133]. To achieve more generic applications, a holographic approach was proposed to generate a desired complex wave-front, which is flexible enough to realize either a 2D or 3D hologram [134]. Comparing to conventional approach of making holograms using discrete depths of materials, the generated phase can be continuously varied in the geometric-phase approach. The holograms generated can now depend on the incident spin and its efficiency can reach nearly 80% by employing a reflection geometry of the metasurface, as shown in Figure 11B and C [134–137].

5.3 Symmetry-related applications with spin-orbit interaction

Symmetry plays a key role in OSHE and symmetry-breaking metasurfaces have shown significant spin-dependent transportation through the strong light-structure interactions. In this way, metasurfaces are providing a very flexible platform to investigate structural symmetry effects. The Rashba effect denotes a splitting of spin-degenerate parabolic bands into bands of opposite spins in the dispersion diagram [138–140]. Such an effect arises from spin-orbit interactions with spatial inversion symmetry broken while the time-reversal symmetry can still be respected. In Section 4, we have seen numerous examples of using a geometric-phase profile to induce a spin-dependent coupling between the incident light and the material. A very useful and alternative perspective is a spin-splitting of the dispersion diagram of the material itself. By exploiting geometric-phase metasurfaces with rotated microstructures [103, 104, 106, 107], an optical counterpart of the Rashba effect can be observed [109–112]. Figure 12A shows a 1D case, in which the structure is rotated from one cell to the next. It causes a spin-splitting of the surface-wave (phonon-polariton) dispersion, which in turns causes a spin-splitting in the absorption spectrum and the thermal radiation bands (see Figure 12A) [108, 109]. A more Rashba-like band structure with spin-split parabolic bands in two dimensions can be obtained using a nanoslot array with rotated orientation angle in a 2D kagome lattice (see Figure 12B) [110]. This spin-dependent coupling between the incident light and the material can be applied to structures of even lower symmetry (e.g. a quasi-crystal) to achieve this Rashba effect [111, 112].

Nonlinear optical processes are also highly sensitive to the symmetry of the nonlinear materials under investigation. For example, second harmonic generations also rely on the absence of inversion centers in the materials or structures. Clearly, the OSHE and the nonlinear optical processes on a 2D metasurface will be intrinsically intertwined. The nonlinear susceptibility tensors of

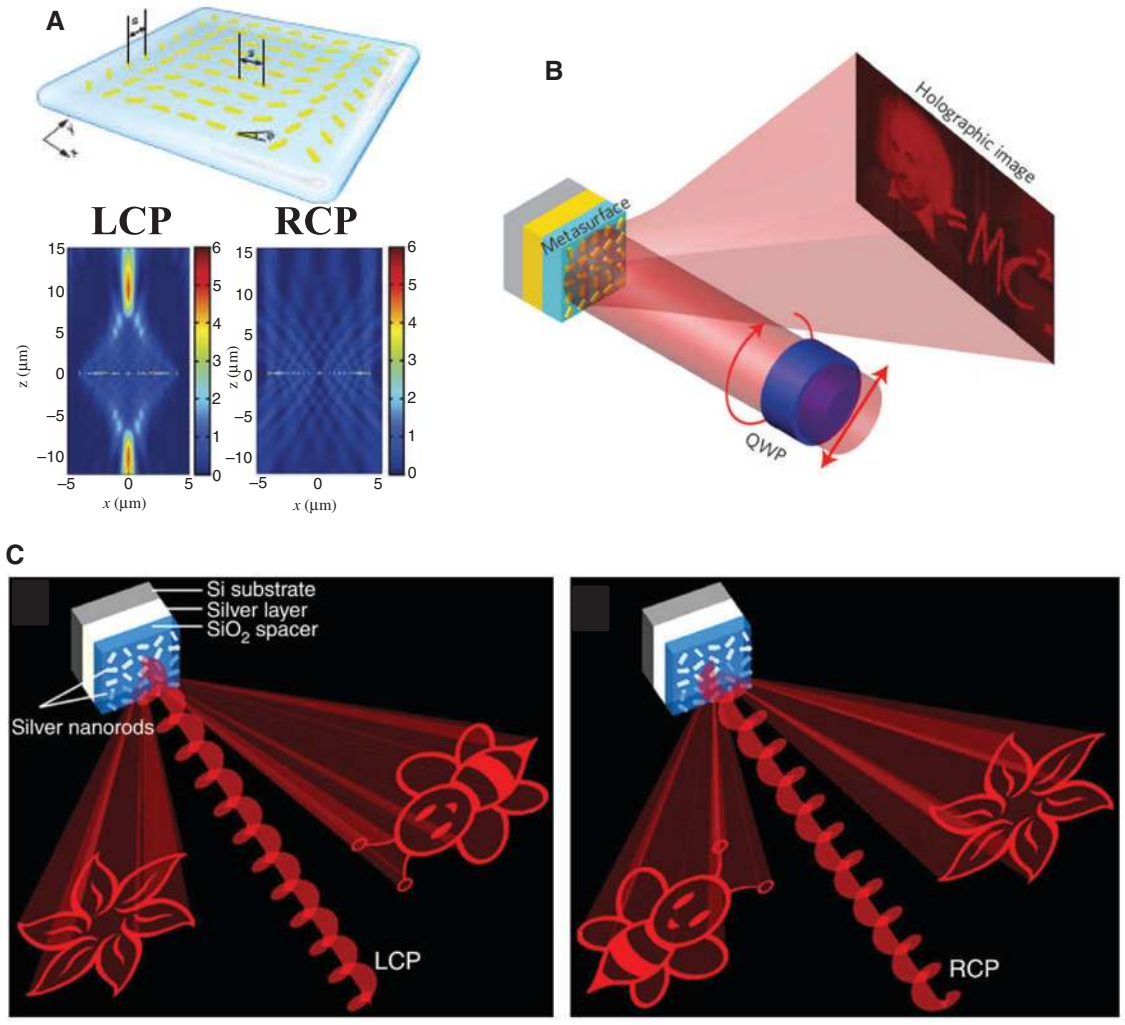

Figure 11: Geometric phase enabled flat optics and hologram.
(A) Dual-polarity plasmonic flat lens for visible light. Reprinted from Ref. [131]. (B) Geometric phase enabled holographic scheme and reconstruction procedure. Reprinted from Ref. [135]. (C) Helicity multiplexed metasurface hologram with dual holographic images. Reprinted from Ref. [136].

the metasurfaces can be easily tailored by the structural design, and the spin state and spectra of the nonlinearly converted light beam can be modulated. Typical examples includes L-shaped gold nanoparticle [142, 143], T-shaped nanoparticle [144], split-ring resonator (SPR) with electric or magnetic dipole resonance [145–147], and silver triangular nanoprisms and nanoholes [148, 149]. A symmetry-breaking metasurface not only significantly enhances its nonlinear optical response but also shows strong spin-selectivity in the nonlinearly generated light [150]. Polarization-dependent selection rules for high harmonic generations on a metasurface have also been extensively studied [151]. As shown in Figure 12C, metasurfaces with two- or four-fold symmetry allow strong third harmonic generation while the process is prohibited in a three-fold symmetric system using a consideration of the geometric phase carried by the plasmonic particle [141, 152]. When these nonlinear particles are arranged into an array with a geometric-phase profile, the spin-orbit interaction dictates the nonlinear susceptibility and alter the spin state and the direction of the nonlinearly converted light through a geometric-phase metasurface (see Figure 12D). Last but not least, secure quantum communication and information processing rely on parametrically generated photon pairs with entangled polarizations states, more explicitly, the entangled spin and/or orbital angular momentum. Metasurfaces with high efficiency in manifesting and detection of photon spin and OAM freedom shall find their applications in quantum information storage, processing, and computation based on the angular and OAM of light.

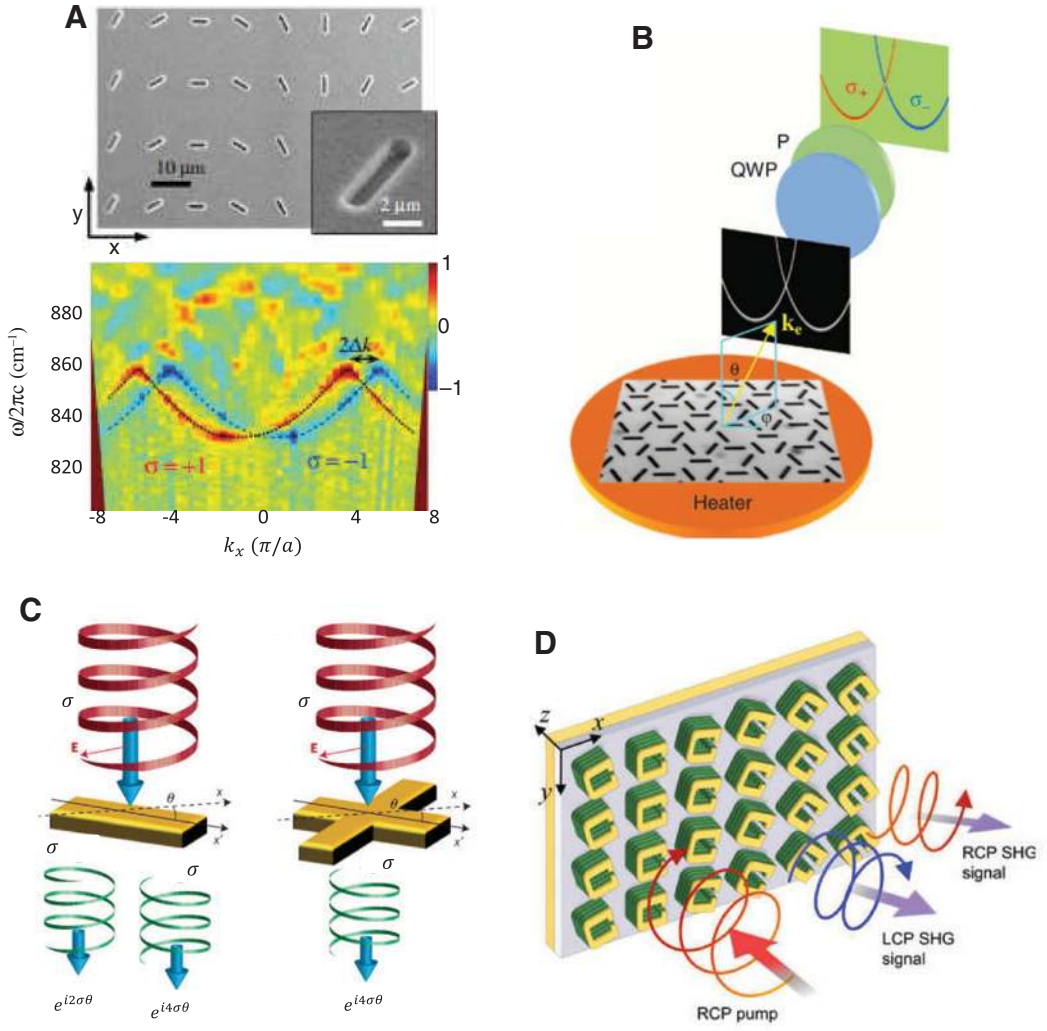

Figure 12: Symmetry effect with spin-orbit interaction.
(A) Spin-split dispersion relation measured by S_3 Stokes parameter of thermal radiation from the rotating slits in one dimension. Reprinted from Ref. [108]. (B) Schematic set-up for the spin-projected dispersion based on 2D Rashba-like metasurface. Reprinted from Ref. [110]. (C) Metasurfaces with two- and four-fold symmetry allows strong third harmonic generation [141]. (D) Geometric-phase profile in selecting the outgoing angle of the second harmonic signal.

6 Conclusions

We have briefly reviewed the fundamental physics and the latest developments in the research field of OSHE enabled by plasmonic structures and metasurfaces. The associated spin-splitting capability from the opposite geometric phases for the opposite spins offers us a versatile approach to spin-dependent optics, allowing us to manipulate both far-field and surface waves. We have also reviewed some potential applications in this field, including spin-dependent beam steering, focusing, structuring, and holograms. We hope by presenting these works together in a concise and coherent way may stimulate further research works using OSHE as the fundamental mechanism.

Acknowledgments: J.L. acknowledges the funding from the European Union's Seventh Framework Programme under grant agreement No. 630979. X.Y. acknowledges the support from the Defense Advanced Research Projects Agency (DARPA) Young Faculty Award under grant number D15AP00106.

References

[1] D'yakonov MI, Perel VI. Optical orientation in a system of electrons and lattice nuclei in semiconductors. Theory Zh Eksp Teor Fiz 1973;65:362–75.
[2] Hirsch JE. Spin Hall effect. Phys Rev Lett 1999;83:1834.

[3] Zhang S. Spin Hall effect in the presence of spin diffusion. Phys Rev Lett 2000;85:393.
[4] Chang MC, Niu Q. Berry phase, hyperorbits, and the Hofstadter spectrum. Phys Rev Lett 1995;75:1348.
[5] Liberman VS, Zel'dovich BY. Spin-orbit interaction of a photon in an inhomogeneous medium. Phys Rev A 1992;46:5199.
[6] Bliokh KY, Bliokh YP. Modified geometrical optics of a smoothly inhomogeneous isotropic medium: the anisotropy, Berry phase, and the optical Magnus effect. Phys Rev E 2004;70:026605.
[7] Bliokh KY, Bliokh YP. Topological spin transport of photons: the optical Magnus effect and Berry phase. Phys Lett A 2004;333:181–6.
[8] Onoda M, Murakami S, Nagaosa N. Hall effect of light. Phys Rev Lett 2004;93:083901.
[9] Onoda M, Murakami S, Nagaosa N. Geometrical aspects in optical wave-packet dynamics. Phys Rev E 2006;74:066610.
[10] Bérard A, Mohrbach H. Spin Hall effect and Berry phase of spinning particles. Phys Lett A 2006;352:190–5.
[11] Bliokh KY. Geometrodynamics of polarized light: Berry phase and spin Hall effect in a gradient-index medium. J Opt A Pure Appl Opt 2009;11:094009.
[12] Bliokh KY, Rodríguez-Fortuño FJ, Nori F, Zayats AV. Spin-orbit interactions of light. Nat Photon 2015;9:796–808.
[13] Gosselin P, Bérard A, Mohrbach H. Spin Hall effect of photons in a static gravitational field. Phys Rev D 2007;75:084035.
[14] Bliokh KY, Freilikher VD. Topological spin transport of photons: magnetic monopole gauge field in Maxwell's equations and polarization splitting of rays in periodically inhomogeneous media. Phys Rev B 2005;72:035108.
[15] Duval C, Horváth Z, Horváthy PA. Fermat principle for spinning light. Phys Rev D 2006;74:021701.
[16] Duval C, Horvath Z, Horváthy PA. Geometrical spin optics and the optical Hall effect. J Geom Phys 2007;57:925–41.
[17] Bliokh KY, Frolov DY, Kravtsov YA. Non-Abelian evolution of electromagnetic waves in a weakly anisotropic inhomogeneous medium. Phys Rev A 2007;75:053821.
[18] Bliokh KY, Niv A, Kleiner V, Hasman E. Geometrodynamics of spinning light. Nat Photon 2008;2:748–53.
[19] Hosten O, Kwiat P. Observation of the spin Hall effect of light via weak measurements. Science 2008;319:787–90.
[20] Zhou X, Xiao Z, Luo H, Wen S. Experimental observation of the spin Hall effect of light on a nanometal film via weak measurements. Phys Rev A 2012;85:043809.
[21] Zhou X, Ling X, Luo H, Wen S. Identifying graphene layers via spin Hall effect of light. Appl Phys Lett 2012;101:251602.
[22] Ross JN. The rotation of the polarization in low birefringence monomode optical fibres due to geometric effects. Opt Quant Electron 1984;16:455–61.
[23] Chiao RY, Wu YS. Manifestations of Berry's topological phase for the photon. Phys Rev Lett 1986;57:933.
[24] Tomita A, Chiao RY. Observation of Berry's topological phase by use of an optical fiber. Phys Rev Lett 1986;57:937.
[25] Haldane FDM. Path dependence of the geometric rotation of polarization in optical fibers. Opt Lett 1986;11:730–2.
[26] Berry MV. Interpreting the anholonomy of coiled light. Nature 1987;326:277–8.
[27] Bomzon Z, Biener G, Kleiner V, Hasman E. Space-variant Pancharatnam-Berry phase optical elements with computer-generated subwavelength gratings. Opt Lett 2002;27:1141–3.
[28] Biener G, Niv A, Kleiner V, Hasman E. Formation of helical beams by use of Pancharatnam-Berry phase optical elements. Opt Lett 2002;27:1875–7.
[29] Hasman E, Bomzon Z, Niv A, Biener G, Kleiner V. Polarization beam-splitters and optical switches based on space-variant computer-generated subwavelength quasi-periodic structures. Opt Commun 2002;209:45–54.
[30] Marrucci L, Manzo C, Paparo D. Pancharatnam-Berry phase optical elements for wave front shaping in the visible domain: switchable helical mode generation. Appl Phys Lett 2006;88:221102.
[31] Marrucci L, Manzo C, Paparo D. Optical spin-to-orbital angular momentum conversion in inhomogeneous anisotropic media. Phys Rev Lett 2006;96:163905.
[32] Ling X, Zhou X, Yi X, et al. Giant photonic spin Hall effect in momentum space in a structured metamaterial with spatially varying birefringence. Light Sci Appl 2015;4:e290.
[33] Shelby RA, Smith DR, Schultz S. Experimental verification of a negative index of refraction. Science 2001;292:77–9.
[34] Smith DR, Pendry JB, Wiltshire MCK. Metamaterials and negative refractive index. Science 2004;305:788–92.
[35] Pendry JB, Schurig D, Smith DR. Controlling electromagnetic fields. Science 2006;312:1780–2.
[36] Leonhardt U. Optical conformal mapping. Science 2006;312:1777–80.
[37] Pendry JB. Negative refraction makes a perfect lens. Phys Rev Lett 2000;85:3966.
[38] Fang N, Lee H, Sun C, Zhang X. Sub-diffraction-limited optical imaging with a silver superlens. Science 2005;308:534–7.
[39] Hao J, Yuan Y, Ran L, et al. Manipulating electromagnetic wave polarizations by anisotropic metamaterials. Phys Rev Lett 2007;99:063908.
[40] Xiao S, Mühlenbernd H, Li G, et al. Helicity-preserving omnidirectional plasmonic mirror. Adv Opt Mater 2016;4:654–8.
[41] Pendry JB. A chiral route to negative refraction. Science 2004;306:1353–5.
[42] Kwon DH, Douglas HW. Polarization splitter and polarization rotator designs based on transformation optics. Opt Express 2008;16:18731–8.
[43] Danner AJ, Tyc T, Leonhardt U. Controlling birefringence in dielectrics. Nat Photon 2011;5:357–9.
[44] Plum E, Zheludev NI. Chiral mirrors. Appl Phys Lett 2015;106:221901.
[45] Yu N, Genevet P, Kats MA, et al. Light propagation with phase discontinuities: generalized laws of reflection and refraction. Science 2011;334:333–7.
[46] Ni X, Emani NK, Kildishev AV, Boltasseva A, Shalaev VM. Broadband light bending with plasmonic nanoantennas. Science 2012;335:427.
[47] Sun S, He Q, Xiao S, Xu Q, Li X, Zhou L. Gradient-index metasurfaces as a bridge linking propagating waves and surface waves. Nat Mater 2012;11:426–31.
[48] Rytov SM. On the transition from wave to geometrical optics. Dokl Akad Nauk SSSR 1938;18:263–7.
[49] Vladimirsky VV. On the rotation of the polarization plane along a curbed ray. Dokl Akad Nauk SSSR 1941;31:222.
[50] Vinitski&ibreve; SI, Derbov VL, Dubovik VM, Markovski BL, Stepanovski&ibreve; YP. Topological phases in quantum

mechanics and polarization optics. Sov Phys Usp 1990;33:403.
[51] Pancharatnam S. Generalized theory of interference and its applications. Proc Indian Acad Sci 1956;44:398–417.
[52] Berry MV. The adiabatic phase and Pancharatnam's phase for polarized light. J Mod Opt 1987;34:1401–7.
[53] Shitrit N, Bretner I, Gorodetski Y, Kleiner V, Hasman E. Optical spin Hall effects in plasmonic chains. Nano Lett 2011;11:2038–42.
[54] Bliokh KY, Gorodetski Y, Kleiner V, Hasman E. Coriolis effect in optics: unified geometric phase and spin-Hall effect. Phys Rev Lett 2008;101:030404.
[55] Gorodetski Y, Niv A, Kleiner V, Hasman E. Observation of the spin-based plasmonic effect in nanoscale structures. Phys Rev Lett 2008;101:043903.
[56] Yin X, Ye Z, Rho J, Wang Y, Zhang X. Photonic spin Hall effect at metasurfaces. Science 2013;339:1405–7.
[57] Aharonov Y, Albert DZ, Vaidman L. How the result of a measurement of a component of the spin of a spin-1/2 particle can turn out to be 100. Phys Rev Lett 1988;60:1351.
[58] Duck IM, Stevenson PM, Sudarshan ECG. The sense in which a "weak measurement" of a spin-1/2 particle's spin component yields a value 100. Phys Rev D 1989:40:2112.
[59] Jozsa R. Complex weak values in quantum measurement. Phys Rev A 2007:76:044103.
[60] Lee YU, Wu JW. Control of optical spin Hall shift in phase-discontinuity metasurface by weak value measurement post-selection. Sci Rep 2015;5:13900.
[61] Ni X, Xiao J, Yang S, Wang Y, Zhang X. Photon spin induced collective electron motion on a metasurface. CLEO: QELS Fundam Sci 2015;FW4E:1.
[62] Li Y, Liu Y, Ling X, et al. Observation of photonic spin Hall effect with phase singularity at dielectric metasurfaces. Opt Express 2015;23:1767–74.
[63] Liu Y, Ling X, Yi X, et al. Photonic spin Hall effect in dielectric metasurfaces with rotational symmetry breaking. Opt Lett 2015;40:756–9.
[64] Bomzon Z, Gu M. Space-variant geometrical phases in focused cylindrical light beams. Opt Lett 2007;32:3017–9.
[65] Shu W, Ke Y, Liu Y, Ling X, Luo H, Yin X. Radial spin Hall effect of light. Phys Rev A 2016;93:013839.
[66] Fedotov VA, Mladyonov PL, Prosvirnin SL, Rogacheva AV, Chen Y, Zheludev NI. Asymmetric propagation of electromagnetic waves through a planar chiral structure. Phys Rev Lett 2006;97:167401.
[67] Kang M, Feng T, Wang HT, Li J. Wave front engineering from an array of thin aperture antennas. Opt Express 2012;20:15882–90.
[68] Huang L, Chen X, Mühlenbernd H, et al. Dispersionless phase discontinuities for controlling light propagation. Nano Lett 2012;12:5750–5.
[69] Liu Z, Chen S, Li J, et al. Fully interferometric controllable anomalous refraction efficiency using cross modulation with plasmonic metasurfaces. Opt Lett 2014;39:6763–6.
[70] Shaltout A, Liu J, Kildishev A, Shalaev V. Photonic spin Hall effect in gap-plasmon metasurfaces for on-chip chiroptical spectroscopy. Optica 2015;2:860–3.
[71] Coullet P, Gil L, Rocca F. Optical vortices. Opt Commun 1989;73:403–8.
[72] Allen L, Beijersbergen MW, Spreeuw RJC, Woerdman JP. Orbital angular momentum of light and the transformation of Laguerre-Gaussian laser modes. Phys Rev A 1992;45:8185.
[73] Allen L, Lembessis VE, Babiker M. Spin-orbit coupling in free-space Laguerre-Gaussian light beams. Phys Rev A 1996;53:R2937.
[74] O'Neil AT, MacVicar I, Allen L, Padgett MJ. Intrinsic and extrinsic nature of the orbital angular momentum of a light beam. Phys Rev Lett 2002;88:053601.
[75] Niv A, Gorodetski Y, Kleiner V, Hasman E. Topological spin-orbit interaction of light in anisotropic inhomogeneous subwavelength structures. Opt Lett 2008;33:2910–2.
[76] Li G, Kang M, Chen S, et al. Spin-enabled plasmonic metasurfaces for manipulating orbital angular momentum of light. Nano Lett 2013;13:4148–51.
[77] Karimi E, Schulz SA, De Leon I, Qassim H, Upham J, Boyd RW. Generating optical orbital angular momentum at visible wavelengths using a plasmonic metasurface. Light Sci Appl 2014;3:e167.
[78] Dong T, Ma X, Mittra R. Modeling large nonuniform optical antenna arrays for metasurface application. J Appl Phys 2013;114:043103.
[79] Ling X, Zhou X, Luo H, Wen S. Steering far-field spin-dependent splitting of light by inhomogeneous anisotropic media. Phys Rev A 2012;86:053824.
[80] Ling X, Zhou X, Shu W, Wen S. Realization of tunable photonic spin Hall effect by tailoring the Pancharatnam-Berry phase. Sci Rep 2014;4:5557.
[81] Ma X, Pu M, Li X, et al. A planar chiral meta-surface for optical vortex generation and focusing. Sci Rep 2015;5:10365.
[82] Ding X, Monticone F, Zhang K, et al. Ultrathin Pancharatnam-Berry metasurface with maximal cross-polarization efficiency. Adv Mater 2015;27:1195–200.
[83] Pfeiffer C, Grbic A. Controlling vector Bessel beams with metasurfaces. Phys Rev Appl 2014;2:044012.
[84] Grady NK, Heyes JE, Chowdhury DR, et al. Terahertz metamaterials for linear polarization conversion and anomalous refraction. Science 2013;340:1304–7.
[85] Luo W, Xiao S, He Q, Sun S, Zhou L. Photonic spin Hall effect with nearly 100% efficiency. Adv Opt Mater 2015;3:11028.
[86] Jiang SC, Xiong X, Hu YS, et al. High-efficiency generation of circularly polarized light via symmetry-induced anomalous reflection. Phys Rev B 2015;91:125421.
[87] Gorodetski Y, Nechayev S, Kleiner V, Hasman E. Plasmonic Aharonov-Bohm effect: optical spin as the magnetic flux parameter. Phys Rev B 2010;82:125433.
[88] Cho SW, Park J, Lee SY, Kim H, Lee B. Coupling of spin and angular momentum of light in plasmonic vortex. Opt Express 2012;20:10083–94.
[89] Kim H, Park J, Cho SW, Lee SY, Kang M, Lee B. Synthesis and dynamic switching of surface plasmon vortices with plasmonic vortex lens. Nano Lett 2010;10:529–36.
[90] Gorodetski Y, Shitrit N, Bretner I, Kleiner V, Hasman E. Observation of optical spin symmetry breaking in nanoapertures. Nano Lett 2009;9:3016–9.
[91] Ohno T, Miyanishi S. Study of surface plasmon chirality induced by Archimedes' spiral grooves. Opt Express 2006;14:6285–90.

[92] Yang S, Chen W, Nelson RL, Zhan Q. Miniature circular polarization analyzer with spiral plasmonic lens. Opt Lett 2009;34:3047–9.
[93] Shen Z, Hu ZJ, Yuan GH, Min CJ, Fang H, Yuan XC. Visualizing orbital angular momentum of plasmonic vortices. Opt Lett 2012;37:4627–9.
[94] Tsai WY, Huang JS, Huang CB. Selective trapping or rotation of isotropic dielectric microparticles by optical near field in a plasmonic Archimedes spiral. Nano Lett 2014;14:547–52.
[95] Ku CT, Lin HN, Huang CB. Direct observation of surface plasmon vortex and subwavelength focusing with arbitrarily-tailored intensity patterns. Appl Phys Lett 2015;106:053112.
[96] Gorodetski Y, Bliokh KY, Stein B, et al. Weak measurements of light chirality with a plasmonic slit. Phys Rev Lett 2012;109:013901.
[97] Lee SY, Lee IM, Park J, et al. Role of magnetic induction currents in nanoslit excitation of surface plasmon polaritons. Phys Rev Lett 2012;108:213907.
[98] Rodríguez-Fortuño FJ, Marino G, Ginzburg P, et al. Near-field interference for the unidirectional excitation of electromagnetic guided modes. Science 2013;340:328–30.
[99] O'Connor D, Ginzburg P, Rodríguez-Fortuño FJ, Wurtz GA, Zayats AV. Spin-orbit coupling in surface plasmon scattering by nanostructures. Nat Commun 2014;5:5327.
[100] Mueller JPB, Capasso F. Asymmetric surface plasmon polariton emission by a dipole emitter near a metal surface. Phys Rev B 2013;88:121410.
[101] Hayat A, Mueller JB, Capasso F. Lateral chirality-sorting optical forces. Proc Natl Acad Sci USA 2015;112:13190–4.
[102] Rodríguez-Fortuño FJ, Engheta N, Martínez A, Zayats AV. Lateral forces on circularly polarizable particles near a surface. Nat Commun 2015;6:8799.
[103] Lin J, Mueller JPB, Wang Q, et al. Polarization-controlled tunable directional coupling of surface plasmon polaritons. Science 2013;340:331–4.
[104] Huang L, Chen X, Bai B, et al. Helicity dependent directional surface plasmon polariton excitation using a metasurface with interfacial phase discontinuity. Light Sci Appl 2013;2:e70.
[105] Xiao S, Zhong F, Liu H, Zhu S, Li J. Flexible coherent control of plasmonic spin-Hall effect. Nat Commun 2015;6:8360.
[106] Genevet P, Wintz D, Ambrosio A, She A, Blanchard R, Capasso F. Controlled steering of Cherenkov surface plasmon wakes with a one-dimensional metamaterial. Nat Nanotechnol 2015;10:804–9.
[107] Du L, Kou SS, Balaur E, et al. Broadband chirality-coded meta-aperture for photon-spin resolving. Nat Commun 2015;6:10051.
[108] Dahan N, Gorodetski Y, Frischwasser K, Kleiner, V, Hasman E. Geometric Doppler effect: spin-split dispersion of thermal radiation. Phys Rev Lett 2010;105:136402.
[109] Shitrit N, Maayani S, Veksler D, Kleiner V, Hasman E. Rashba-type plasmonic metasurface. Opt Lett 2013;38:4358–61.
[110] Shitrit N, Yulevich I, Maguid E, et al. Spin-optical metamaterial route to spin-controlled photonics. Science 2013;340:724–6.
[111] Shitrit N, Yulevich I, Kleiner V, Hasman E. Spin-controlled plasmonics via optical Rashba effect. Appl Phys Lett 2013;103:211114.
[112] Yulevich I, Maguid E, Shitrit N, Veksler D, Kleiner V, Hasman E. Optical mode control by geometric phase in quasicrystal metasurface. Phys Rev Lett 2015;115:205501.
[113] Pors A, Nielsen MG, Bozhevolnyi SI. Plasmonic metagratings for simultaneous determination of Stokes parameters. Optica 2015;2:716–23.
[114] Wen D, Yue F, Kumar S, et al. Metasurface for characterization of the polarization state of light. Opt Express 2015;23:10272–81.
[115] Yang Y, Wang W, Moitra P, Kravchenko II, Briggs DP, Valentine J. Dielectric meta-reflectarray for broadband linear polarization conversion and optical vortex generation. Nano Lett 2014;14:1394–9.
[116] Zhang J, MacDonald KF, Zheludev NI. Controlling light-with-light without nonlinearity. Light Sci Appl 2012;1:e18.
[117] Mousavi SA, Plum E, Shi J, Zheludev NI. Coherent control of birefringence and optical activity. Appl Phys Lett 2014;105:011906.
[118] Shi J, Fang X, Rogers ETF, Plum E, MacDonald KF, Zheludev NI. Coherent control of Snell's law at metasurfaces. Opt Express 2014;22:21051–60.
[119] Torner L, Torres JP, Carrasco S. Digital spiral imaging. Opt Express 2005;13:873–81.
[120] Monroe D. Focus: big twist for electron beam. Physics 2015;8:7.
[121] Oemrawsingh SSR, Van Houwelingen JAW, Eliel ER, Woerdman JP, Verstegen EJK, Kloosterboer JG. Production and characterization of spiral phase plates for optical wavelengths. Appl Opt 2004;43:688–94.
[122] Savage N. Digital spatial light modulators. Nat Photon 2009;3:170–2.
[123] Chen L, Lei J, Romero J. Quantum digital spiral imaging. Light Sci Appl 2014;3:e153.
[124] Ghai DP, Senthilkumaran P, Sirohi RS. Single-slit diffraction of an optical beam with phase singularity. Opt Laser Eng 2009;47:123–6.
[125] Sztul HI, Alfano RR. Double-slit interference with Laguerre-Gaussian beams. Opt Lett 2006;31:999–1001.
[126] Fischer P, Skelton SE, Leburn CG, Streuber CT, Wright EM, Dholakia K. Propagation and diffraction of optical vortices. Physica C 2008;468:514–7.
[127] Leach J, Padgett MJ, Barnett SM, Franke-Arnold S, Courtial J. Measuring the orbital angular momentum of a single photon. Phys Review Lett 2002;88:257901.
[128] Genevet P, Lin J, Kats MA, Capasso F. Holographic detection of the orbital angular momentum of light with plasmonic photodiodes. Nat Commun 2012;3:1278.
[129] Liu AP, Xiong X, Ren XF, et al. Detecting orbital angular momentum through division-of-amplitude interference with a circular plasmonic lens. Sci Rep 2013;3:2402.
[130] Liu A, Rui G, Ren X, Zhan Q, Guo G, Guo G. Encoding photonic angular momentum information onto surface plasmon polaritons with plasmonic lens. Opt Express 2012;20:24151–9.
[131] Chen X, Huang L, Mühlenbernd H, et al. Dual-polarity plasmonic metalens for visible light. Nat Commun 2012;3:1198.
[132] Wang W, Guo Z, Li R, et al. Plasmonics metalens independent from the incident polarizations. Opt Express 2015;23:16782–91.
[133] Huang K, Li Y, Tian X, Zeng D, Gao X. Design and analyses of an ultra-thin flat lens for wave front shaping in the visible. Phys Lett A 2015;379:3008–12.
[134] Huang L, Chen X, Mühlenbernd H, et al. Three-dimensional optical holography using a plasmonic metasurface. Nat Commun 2013;4:2808.

[135] Zheng G, Mühlenbernd H, Kenney M, Li G, Zentgraf T, Zhang S. Metasurface holograms reaching 80% efficiency. Nat Nanotechnol 2015;10:308–12.
[136] Wen D, Yue F, Li G, et al. Helicity multiplexed broadband metasurface holograms. Nat Commun 2015;6:8241.
[137] Ni X, Kildishev AV, Shalaev VM. Metasurface holograms for visible light. Nat Commun 2013;4:2807.
[138] Dresselhaus G. Spin-orbit coupling effects in zinc blend structures. Phys Rev 1955;100:580.
[139] Rashba EI. Properties of semiconductors with an extremum loop. 1. Cyclotron and combinational resonance in a magnetic field perpendicular to the plane of the loop. Sov Phys Solid State 1960;2:1109–22.
[140] Ishizaka K, Bahramy MS, Murakawa H, et al. Giant Rashba-type spin splitting in bulk BiTeI. Nat Mater 2011;10:521–6.
[141] Chen S, Li G, Zeuner F, et al. Symmetry-selective third-harmonic generation from plasmonic metacrystals. Phys Rev Lett 2014;11:033901.
[142] Tuovinen H, Kauranen M, Jefimovs K, et al. Linear and second-order nonlinear optical properties of arrays of noncentrosymmetric gold nanoparticles. J Nonlinear Opt Phys 2002;11:421–32.
[143] Canfield BK, Kujala S, Jefimovs K, Turunen J, Kauranen M. Linear and nonlinear optical responses influenced by broken symmetry in an array of gold nanoparticles. Opt Express 2004;12:5418–23.
[144] Canfield BK, Husu H, Laukkanen J, et al. Local field asymmetry drives second-harmonic generation in noncentrosymmetric nanodimers. Nano Lett 2007;7:1251–5.
[145] Feth N, Linden S, Klein MW, et al. Second-harmonic generation from complementary split-ring resonators. Opt Lett 2008;33:1975–7.
[146] Niesler FBP, Feth N, Linden S, Wegener M. Second-harmonic optical spectroscopy on split-ring-resonator arrays. Opt Lett 2011;36:1533–5.
[147] Klein MW, Enkrich C, Wegener M, Linden S. Second-harmonic generation from magnetic metamaterials. Science 2006;313:502–4.
[148] Salomon A, Zielinski M, Kolkowski R, Zyss J, Prior Y. Size and shape resonances in second harmonic generation from silver nanocavities. J Phys Chem C 2013;117:22377–82.
[149] Singh AK, Senapati D, Neely A, Kolawole G, Hawker C, Ray PC. Nonlinear optical properties of triangular silver nanomaterials. Chem Phys Lett 2009;481:94–8.
[150] Konishi K, Higuchi T, Li J, Larsson J, Ishii S, Kuwata-Gonokami M. Polarization-controlled circular second-harmonic generation from metal hole arrays with threefold rotational symmetry. Phys Rev Lett 2014;112:135502.
[151] Alon OE, Averbukh V, Moiseyev N. Selection rules for the high harmonic generation spectra. Phys Rev Lett 1998;80:3743.
[152] Li G, Chen S, Pholchai N, et al. Continuous control of the nonlinearity phase for harmonic generations. Nat Mater 2015;14:607–12.